Steady low Mach number flows: identification of the spurious mode and filtering method

Jonathan Jung, Vincent Perrier

▶ **To cite this version:**

Jonathan Jung, Vincent Perrier. Steady low Mach number flows: identification of the spurious mode and filtering method. Journal of Computational Physics, 2022, pp.111462. 10.1016/j.jcp.2022.111462 . hal-03736193

HAL Id: hal-03736193
https://hal.science/hal-03736193

Submitted on 22 Jul 2022

HAL is a multi-disciplinary open access archive for the deposit and dissemination of scientific research documents, whether they are published or not. The documents may come from teaching and research institutions in France or abroad, or from public or private research centers.

L'archive ouverte pluridisciplinaire **HAL**, est destinée au dépôt et à la diffusion de documents scientifiques de niveau recherche, publiés ou non, émanant des établissements d'enseignement et de recherche français ou étrangers, des laboratoires publics ou privés.

Steady low Mach number flows : identification of the spurious mode and filtering method

Jonathan Jung* and Vincent Perrier†

Cagire team, Inria BSO and LMAP, UPPA, E2S UPPA, CNRS, Pau, France
avenue de l'Université, 64013 Pau Cedex

Abstract

The aim of this article is to thoroughly identify the spurious mode that jeopardizes the convergence of usual upwind numerical schemes for compressible flows when the Mach number goes to 0. We show that this spurious mode is the long time limit of a wave system whose properties and discretization depend on the scheme used for the compressible system. Once this spurious mode is identified, a filtering method is developed for removing it from the solution of stationary low Mach number compressible flow. Numerical results confirm that at the price of the computation of a long time solution of the wave system, the accuracy of an inaccurate solution of a low Mach number compressible flow can be greatly improved by this filtering method.

Keywords — Low Mach compressible flows, Density based solvers, Finite volume methods, Euler equations.

Contents

*Corresponding author. Email: **jonathan.jung@univ-pau.fr**
†Email: **vincent.perrier@inria.fr**.

1 Introduction

We consider the isentropic Euler model

$$\begin{cases} \partial_t \rho + \nabla \cdot (\rho \mathbf{u}) = 0, \\ \partial_t (\rho \mathbf{u}) + \nabla \cdot (\rho \mathbf{u} \otimes \mathbf{u}) + \nabla p = 0, \end{cases} \tag{1}$$

where ρ is the density, p the pressure, and $\mathbf{u}$ the velocity. The problem is solved on a domain Ω. For closing the system, the pressure is supposed to depend only on ρ: $p = p(\rho)$. Assume that p is a convex function of ρ. Under these assumptions, this system is well-known to be hyperbolic with eigenvalues in the direction $\mathbf{n}$ given by $\lambda_\pm = \mathbf{u} \cdot \mathbf{n} \pm a$, where the sound speed a is given by $a(\rho) = \sqrt{p'(\rho)}$, with genuinely nonlinear characteristic fields and $\lambda = \mathbf{u} \cdot \mathbf{n}$ of multiplicity $d-1$ where $d \in \{1, 2, 3\}$ is the space dimension, with linear characteristic fields. Equations (1) can be written in the conservative form

$$\partial_t \mathbf{W} + \nabla \cdot \mathbf{f}(\mathbf{W}) = 0, \tag{2}$$

where $\mathbf{W} = (\rho, \rho\mathbf{u})^T$ is the vector of conservative variables and $\mathbf{f}$ is the flux, given in dimension d by

$$\mathbf{f}(\mathbf{W}) = \begin{pmatrix} \rho \mathbf{u} \\ \rho \mathbf{u} \otimes \mathbf{u} + p \mathrm{I} \end{pmatrix}.$$

This paper deals with flow on a bounded domain. This means that a density ρ_b and a velocity $\mathbf{u}_b$ are (weakly) imposed on the boundary of the domain $\partial\Omega$. In particular, we will consider two types of boundary conditions: wall, and inlet/outlet. For a wall boundary condition, we impose the flux

$$F^{\mathrm{wall}}(\mathbf{W}, \mathbf{n}) = F^{\mathrm{Roe}}(\mathbf{W}, \widetilde{\mathbf{W}}, \mathbf{n}) \tag{3a}$$

where the flux F^{Roe} corresponds to the Roe numerical flux (see subsection A.2) and $\widetilde{\mathbf{W}}$ is obtained from the transformation of $\mathbf{W}$: $\widetilde{\mathbf{W}} = (\mathrm{I}_{d+1} - P_{\mathrm{wall}}(\mathbf{n}))\mathbf{W}$ with

$$P_{\mathrm{wall}}(\mathbf{n}) = \begin{pmatrix} 0 & 0 \\ 0 & 2\mathbf{n}\mathbf{n}^T \end{pmatrix}.$$

For inlet/outlet boundary condition, we impose the modified Steger-Warming flux

$$F^{\mathrm{SW}}(\mathbf{W}, \mathbf{W}_b, \mathbf{n}) = A^+(\mathbf{W}_b, \mathbf{n})\mathbf{W} + A^-(\mathbf{W}_b, \mathbf{n})\mathbf{W}_b, \tag{3b}$$

where A^+ and A^- are respectively the positive and negative parts of the Jacobian matrix of the flux $\mathbf{f}$. For more details on the boundary conditions, we refer to subsection A.3 and subsection A.4.

For studying the behavior of system (1) in the low Mach number regime, three characteristic scales are supposed to be known: a length scale x_0, a density scale ρ_0 and a velocity scale u_0. Then the following dimensionless variables may be defined

$$\tilde{\mathbf{x}} = \frac{\mathbf{x}}{x_0}, \qquad \tilde{\rho} = \frac{\rho}{\rho_0} \qquad \tilde{\mathbf{u}} = \frac{\mathbf{u}}{u_0}. \tag{4}$$

It is natural to scale the time by $t_0 = x_0/u_0$, and the pressure by $p_0 = p(\rho_0)$, and also to define $a_0^2 = p'(\rho_0)$. If the corresponding dimensionless variables are used instead of the original ones, the

following system is obtained

$$\begin{cases} \partial_{\tilde{t}}\tilde{\rho} + \nabla_{\tilde{\mathbf{x}}} \cdot (\tilde{\rho}\tilde{\mathbf{u}}) = 0 \\ \partial_{\tilde{t}}(\tilde{\rho}\tilde{\mathbf{u}}) + \nabla_{\tilde{\mathbf{x}}} \cdot (\tilde{\rho}\tilde{\mathbf{u}} \otimes \tilde{\mathbf{u}}) + \dfrac{1}{\gamma M^2} \nabla_{\tilde{\mathbf{x}}} \tilde{p} = 0, \end{cases} \tag{5}$$

with $\tilde{t} = t/t_0$, $\tilde{p} = p/p_0$, $\tilde{p}(\tilde{\rho}) := p(\rho_0\tilde{\rho})/p_0$, and $M = u_0/a_0$. The coefficient γ is defined as

$$\gamma = \frac{\rho_0 a_0^2}{p_0} = \tilde{p}'(1).$$

The dimensionless boundary fluxes $\tilde{F}^{\text{wall}}\left(\tilde{\mathbf{W}}, \mathbf{n}, M\right)$ and $\tilde{F}^{\text{SW}}\left(\tilde{\mathbf{W}}, \tilde{\mathbf{W}}_b, \mathbf{n}, M\right)$ are detailed in subsection A.3 and subsection A.4.

We assume that the initial condition and the boundary condition are *well prepared* [24, p.641] in the sense that

$$\begin{cases} \tilde{\rho}(\tilde{\mathbf{x}}, \tilde{t} = 0, M) = \tilde{\rho}^{(0)} + \mathcal{O}\left(M^2\right), \\ \tilde{\mathbf{u}}(\tilde{\mathbf{x}}, \tilde{t} = 0, M) = \tilde{\mathbf{u}}^{(0)}(\tilde{\mathbf{x}}) + \mathcal{O}\left(M\right), \end{cases} \quad \text{where} \quad \begin{cases} \tilde{\rho}^{(0)}(\tilde{\mathbf{x}}) = \tilde{\rho}^{(0)} \in \mathbb{R}^+, \\ \nabla_{\tilde{\mathbf{x}}} \cdot (\tilde{\mathbf{u}}^{(0)}) = 0, \end{cases} \tag{6a}$$

and the values ρ_b and $\mathbf{u}_b$ in (3b) satisfy

$$\tilde{\rho}_b(\tilde{\mathbf{x}}, \tilde{t}, M) = \tilde{\rho}^{(0)} + \mathcal{O}\left(M^2\right), \tag{6b}$$

and

$$\tilde{\mathbf{u}}_b(\tilde{\mathbf{x}}, \tilde{t}, M) = \tilde{\mathbf{u}}_b^{(0)}(\tilde{t}) + \mathcal{O}\left(M\right). \tag{6c}$$

Injecting an expansion in exponent of the Mach number M in (5), we get that, if the initial condition and the boundary condition are well prepared (6), the low Mach number limit density fluctuation scales as $\mathcal{O}\left(M^2\right)$ [24].

It is well known [19] that in general classical finite volume methods for (1) are not accurate in the low Mach number limit because it introduces a spurious mode in $\mathcal{O}\left(M\right)$ on the density fluctuations, and that fixes are required for recovering an acceptable accuracy.

The spurious mode is due to an excessive numerical diffusion of the scheme. Some fixes have been derived by modifying the numerical diffusion of the finite volume schemes [19, 25, 26, 12, 32, 14, 29, 7, 21], the Riemann solver is partially replaced by a central difference approximation for the pressure gradient. In this sense, low Mach fixes are similar to schemes based on specific semi-implicit (e.g. IMEX) time discretization [10, 11, 8, 20, 23, 3, 4]. Semi-implicit solvers use central difference approximation for the pressure gradient because it makes the implicit time integration easier. Indeed, it allows to decouple the computation of the density field from the velocity field. These two approaches have their limitations because a central difference approximation for the pressure gradient does not allow to solve accurately the low Mach number acoustic waves [5], in particular when the acoustic wave corresponds to a perturbation of order $\mathcal{O}\left(M\right)$ on the density and of order $\mathcal{O}\left(1\right)$ on the velocity (note that in this particular case the initial and boundary conditions are not *well prepared*). Indeed, in such a wave, a second order scheme with a central difference approximation for the pressure gradient provides only a first order on the moments [5].

Recently, low Mach fixes leading to a decentered discretization of the pressure gradient have been proposed in [5, 2]. However, we note that the fix of [5] is not Galilean invariant while the fix of [2] is developed only for Cartesian meshes.

Our aim in this article is slightly different: we do not want to propose a new finite volume fix but we wish to characterize the spurious mode responsible for the low accuracy when the Mach number goes to 0. An important step is to understand the link between the long time behavior of the wave system and the low Mach number limit of (5), which is developed in section 2 for the continuous case, and in section 3 for the discrete case.

Once the spurious mode of the numerical scheme at the low Mach number limit is well identified, it is possible to remove it. We thus propose in section 4 a numerical method for using the associated numerical long time limit of the wave system to filter the numerical solution of the compressible system at low Mach number. We test this method in section 5, and prove that this method allows to transform a low accurate low Mach number solution into a highly accurate low Mach number solution. The filtering method is rather viewed as a way to validate the identification of the spurious mode than as a numerical method itself. Indeed, to compute low Mach number steady flows, we could directly use preconditioning techniques (e.g. [35, 36]).

2 Link between the long time behavior of the wave system and the low Mach number limit: the continuous case

In [34, Theorem 3.1] a rigorous proof of a link between the low Mach number expansion of the solution of (5) and a wave system was provided: the first order pressure and the zeroth order velocity are indeed solution of a wave system. From this, the uniformity of the first order pressure and the vanishing divergence of the zeroth order velocity can be proven. The proof of [34] is done in the unbounded case and relies on the Fourier analysis, which can hardly be extended to the bounded case. In this section, we aim at doing formally the same link, but in the bounded case.

2.1 Two-scale asymptotic expansion of the continuous system

A two time scales asymptotic expansion of the system (5) is performed as in [27]. The two time scales are the material time $\tilde{t}$ and the acoustic time $\tau = \tilde{t}/M$. We write $\tilde{\varphi} \in \{\rho, \rho\mathbf{u}\}$ as an expansion in exponent of the Mach number M:

$$\tilde{\varphi}(\tilde{\mathbf{x}}, \tilde{t}; M) = \sum_{n=0}^{N} M^n \tilde{\varphi}^{(n)}(\tilde{\mathbf{x}}, \tilde{t}, \tau) + \mathcal{O}\left(M^{N+1}\right), \tag{7}$$

with $\tau = \tilde{t}/M$ and where the derivative with respect to the time is

$$\partial_{\tilde{t}}\tilde{\varphi}\left(\tilde{\mathbf{x}}, \tilde{t}; M\right) = \sum_{n=0}^{N} M^n \left(\partial_{\tilde{t}}\tilde{\varphi}^{(n)}(\tilde{\mathbf{x}}, \tilde{t}, \tau) + \frac{1}{M}\,\partial_{\tau}\tilde{\varphi}^{(n)}(\tilde{\mathbf{x}}, \tilde{t}, \tau)\right) + \mathcal{O}\left(M^{N+1}\right). \tag{8}$$

By injecting (7) in (5), it can be proven that $\tilde{\rho}^{(0)}$ does not depend on τ and $\tilde{\mathbf{x}}$, but only on $\tilde{t}$, and that the following system coupling $\tilde{\rho}^{(1)}$ and $(\tilde{\rho}\tilde{\mathbf{u}})^{(0)}$ holds

$$\begin{cases} \partial_{\tau}\tilde{\rho}^{(1)} + \nabla_{\tilde{\mathbf{x}}} \cdot (\tilde{\rho}\tilde{\mathbf{u}})^{(0)} = -\dfrac{\mathrm{d}\tilde{\rho}^{(0)}}{\mathrm{d}\tilde{t}} \\ \partial_{\tau}\left(\tilde{\rho}\tilde{\mathbf{u}}\right)^{(0)} + \dfrac{\tilde{p}'\left(\tilde{\rho}^{(0)}\right)}{\gamma}\nabla_{\tilde{\mathbf{x}}}\tilde{\rho}^{(1)} = 0 \end{cases} \tag{9}$$

Using the equation of state gives

$$\frac{\tilde{p}'\left(\tilde{\rho}^{(0)}\right)}{\gamma} = \frac{p_0}{\rho_0 a_0^2}\frac{\rho_0}{p_0}\,p'\left(\rho_0\tilde{\rho}^{(0)}\right) = \frac{p'\left(\rho_0\tilde{\rho}^{(0)}\right)}{a_0^2} = \frac{a^2\left(\rho_0\tilde{\rho}^{(0)}\right)}{a_0^2} = \tilde{a}^2\left(\tilde{\rho}^{(0)}\right), \tag{10}$$

so that provided $\tilde{\rho}^{(0)}$ is constant, (9) can be rewritten

$$\begin{cases} \partial_{\tau}\tilde{\rho}^{(1)} + \nabla_{\tilde{\mathbf{x}}} \cdot (\tilde{\rho}\tilde{\mathbf{u}})^{(0)} = 0 \\ \partial_{\tau}\left(\tilde{\rho}\tilde{\mathbf{u}}\right)^{(0)} + \tilde{a}^2\left(\tilde{\rho}^{(0)}\right)\nabla_{\tilde{\mathbf{x}}}\tilde{\rho}^{(1)} = 0. \end{cases} \tag{11}$$

Since the initial and boundary conditions are *well prepared* (6), the initial condition for (11) is given by

$$\begin{cases} \tilde{\rho}^{(1)}(\tilde{\mathbf{x}}, \tau = 0) = 0, \\ (\tilde{\rho}\tilde{\mathbf{u}})^{(0)}(\tilde{\mathbf{x}}, \tau = 0) = \tilde{\rho}^{(0)}\tilde{\mathbf{u}}^{(0)}(\tilde{\mathbf{x}}), \end{cases} \qquad \text{where} \qquad \nabla_{\tilde{\mathbf{x}}} \cdot (\tilde{\rho}^{(0)}\tilde{\mathbf{u}}^{(0)}) = 0, \tag{12a}$$

and the boundary fluxes are given by

$$\begin{bmatrix} (\tilde{\rho}\tilde{\mathbf{u}})^{(0)} \cdot \mathbf{n} \\ \tilde{a}^2\left(\tilde{\rho}^{(0)}\right)\tilde{\rho}^{(1)}\mathbf{n} \end{bmatrix}_{\text{wall}} = \begin{pmatrix} 0 \\ \tilde{a}^2\left(\tilde{\rho}^{(0)}\right)\tilde{\rho}^{(1)}\mathbf{n} + \tilde{a}(\tilde{\rho}^{(0)})\left((\tilde{\rho}\tilde{\mathbf{u}})^{(0)} \cdot \mathbf{n}\right)\mathbf{n} \end{pmatrix} \tag{12b}$$

for a wall boundary condition and

$$\begin{bmatrix} (\tilde{\rho}\tilde{\mathbf{u}})^{(0)} \cdot \mathbf{n} \\ \tilde{a}^2\left(\tilde{\rho}^{(0)}\right)\tilde{\rho}^{(1)}\mathbf{n} \end{bmatrix}_{\text{SW}} = \begin{pmatrix} \dfrac{(\tilde{\rho}\tilde{\mathbf{u}})^{(0)} \cdot \mathbf{n} + (\tilde{\rho}\tilde{\mathbf{u}})_b^{(0)} \cdot \mathbf{n}}{2} + \dfrac{\tilde{a}(\tilde{\rho}^{(0)})}{2}(\tilde{\rho}^{(1)} - 0) \\ \tilde{a}^2\left(\tilde{\rho}^{(0)}\right)\dfrac{\tilde{\rho}^{(1)} + 0}{2}\mathbf{n} + \dfrac{\tilde{a}(\tilde{\rho}^{(0)})}{2}\left((\tilde{\rho}\tilde{\mathbf{u}})^{(0)} \cdot \mathbf{n} - (\tilde{\rho}\tilde{\mathbf{u}})_b^{(0)} \cdot \mathbf{n}\right)\mathbf{n} \end{pmatrix} \tag{12c}$$

for inlet/outlet boundary condition.

2.2 Formal link between the low Mach number behavior and the long time limit of the wave system

The system (11) belongs to the larger family of first order waves systems, which reads

$$\begin{cases} \partial_\tau \widehat{p} + \dfrac{1}{\widehat{\rho_0}} \mathrm{div}_{\mathbf{x}} \widehat{\mathbf{u}} = 0 \\ \partial_\tau \widehat{\mathbf{u}} + \widehat{\kappa_0} \nabla \widehat{p} = 0 \end{cases} \tag{13}$$

depending on two strictly non-negative parameters, $\widehat{\kappa_0}$ and $\widehat{\rho_0}$. The wave velocity is $\widehat{c_0}$, linked with the parameters of the system by $\widehat{c_0}^2 = \widehat{\kappa_0}/\widehat{\rho_0}$. In particular, we note that system (11) can be written as system (13) with $\widehat{\rho_0} = 1$ and $\widehat{\kappa_0} = \tilde{a}^2(\tilde{\rho}^{(0)})$ such that $\widehat{c_0} = \tilde{a}(\tilde{\rho}^{(0)})$. The initial and boundary conditions (12) lead us to study system (13) with the following initial condition

$$\begin{cases} \widehat{p}(\mathbf{x}, \tau = 0) = 0, \\ \widehat{\mathbf{u}}(\mathbf{x}, \tau = 0) = \widehat{\mathbf{u}}_0(\mathbf{x}) \end{cases} \qquad \text{where} \qquad \mathrm{div}_{\mathbf{x}} \widehat{\mathbf{u}}_0 = 0 \tag{14a}$$

and with the following boundary fluxes:

$$\begin{bmatrix} \dfrac{1}{\widehat{\rho_0}} \widehat{\mathbf{u}} \cdot \mathbf{n} \\ \widehat{\kappa_0} \widehat{p} \mathbf{n} \end{bmatrix}_{\text{wall}} = \begin{pmatrix} 0 \\ \widehat{\kappa_0} \widehat{p} \mathbf{n} + \widehat{c_0} (\widehat{\mathbf{u}} \cdot \mathbf{n}) \mathbf{n} \end{pmatrix} \tag{14b}$$

for wall boundary condition and

$$\begin{bmatrix} \dfrac{1}{\widehat{\rho_0}} \widehat{\mathbf{u}} \cdot \mathbf{n} \\ \widehat{\kappa_0} \widehat{p} \mathbf{n} \end{bmatrix}_{\text{SW}} = \begin{pmatrix} \dfrac{1}{\widehat{\rho_0}} \dfrac{\widehat{\mathbf{u}} \cdot \mathbf{n} + \widehat{\mathbf{u}}_b \cdot \mathbf{n}}{2} + \dfrac{\widehat{c_0}}{2} (\widehat{p} - 0) \\ \widehat{\kappa_0} \dfrac{\widehat{p} + 0}{2} \mathbf{n} + \dfrac{\widehat{c_0}}{2} (\widehat{\mathbf{u}} \cdot \mathbf{n} - \widehat{\mathbf{u}}_b \cdot \mathbf{n}) \mathbf{n} \end{pmatrix} \tag{14c}$$

for inlet/outlet boundary condition.

As we are interested in the limit when $M \to 0$, and considering that $\tau = \tilde{t}/M$, it is natural to be interested in the long time limit of (13). If the derivatives with respect to τ vanish, this gives $\nabla \widehat{p} = 0$, so that $\widehat{p}$ is uniform. Considering (6), the boundary pressure of (13) is $\widehat{p}_b = 0$, so that the long time pressure $\widehat{p}$ is uniformly 0. The fact that the long time pressure is 0 can be rewritten as $\tilde{\rho}^{(1)} = 0$, so that

$$\tilde{\rho}(\tilde{\mathbf{x}}, \tilde{t}) = \tilde{\rho}^{(0)} + \mathcal{O}\left(M^2\right),$$

which means that the pressure fluctuations should scale as M^2. Concerning the velocity, the problem is slightly more complicated and developed in the next section.

2.3 A Hodge-Helmholtz decomposition adapted to the long time study of the wave system

The Hodge-Helmholtz decomposition was used in the analysis of low Mach number flows [15] in periodic or infinite domains. In the bounded case, this decomposition depends on the boundary conditions imposed. We provide here a Hodge-Helmholtz decomposition that will be adapted to the analysis in a bounded domain.

Proposition 1 (Hodge-Helmholtz decomposition)**.** *If Ω is such that $\mathrm{Tr}(H^s(\Omega)) \subset H^{s-1/2}(\partial\Omega)$, then any $\mathbf{u} \in (L^2(\Omega))^d$ can be uniquely decomposed as*

$$\begin{cases} \mathbf{u} = \mathbf{u}_\varphi + \mathbf{u}_\Psi & \text{in } \Omega \\ \mathbf{u}_\varphi \cdot \mathbf{n} = \mathbf{u} \cdot \mathbf{n} - \mathbf{u}_b \cdot \mathbf{n} & \text{in } \partial\Omega \end{cases} \tag{15}$$

where $\mathbf{u}_\varphi \in \nabla_{\mathbf{x}} \left(H^1(\Omega)\right)$ and $\mathbf{u}_\Psi \in \mathbf{curl}_{\mathbf{x}} \left(\left(H^1(\Omega)\right)^d\right)$.

The proof of this proposition was deferred to subsection B.1. We say that the Hodge-Helmholtz decomposition proposed in Proposition 1 is adapted to the study of the long time limit of (13), because if a solution has initially a uniform pressure equal to the boundary pressure imposed, and an initial velocity such that $\mathbf{u}_\varphi = 0$, then this solution is not changed by the wave system. More precisely,

Proposition 2. *Consider a solution of the wave system (13) with initial and boundary conditions given by (14). Then it has a limit when $t \to \infty$, and this limit has a uniform pressure, equal to $\widehat{p}_b$, and the velocity tends to $\widehat{\mathbf{u}}_{\mathbf{\Psi}}(0)$ where $\widehat{\mathbf{u}}_{\mathbf{\Psi}}(0)$ corresponds to the divergence free component of the Hodge-Helmholtz decomposition (15) of the initial condition $\widehat{\mathbf{u}}_0$.*

The proof of this proposition is deferred to subsection B.2. Proposition 2 implies that if $\widehat{\mathbf{u}}$ is initially curl free, then $\widehat{\mathbf{u}}$ is curl free for all time, and so $\widehat{\mathbf{u}}$ is harmonic. Therefore the same result as in [34] holds formally.

3 Discrete case

In this section, we aim at doing a similar analysis as in the previous section, but in the discrete case with a finite volume method.

It is worth noting that the discrete unbounded case was investigated in [1], by using the same tool as in [34], the Fourier transform, which can be used only in the unbounded case and concerning the discrete case on Cartesian meshes.

3.1 Asymptotic consistency with the finite volume discretization of the wave system

The aim of this section is to show that with a formal asymptotic development, the discrete problem of the low Mach number limit is also linked with the long time behavior of a discretization of the wave system.

3.1.1 The finite volume scheme

We consider a discretization of (1). The domain is supposed to be bounded, and $\mathcal{T}_h$ denotes a mesh of this domain, on which a cell-centered finite volume discretization is applied. For a given cell i of $\mathcal{T}_h$, we denote by $\mathcal{V}_{\text{int}}(i)$ the set of the neighbors of the cell i, by $\mathcal{V}_{\text{wall}}(i)$ the set of the boundary sides of i on which wall boundary conditions are imposed, and by $\mathcal{V}_{\text{SW}}(i)$ the set of the boundary sides of i on which inlet/outlet Steger-Warming boundary conditions are imposed. Also, we denote by $|\Omega_i|$ the volume of the cell i, by $|\Gamma_{ij}|$ the size of the side linking ij, and by $\mathbf{n}_{ij}$ the unit normal outgoing from i. The finite volume discretization of (1) reads for cell i

$$\begin{aligned}\partial_t \mathbf{W}_i + \frac{1}{|\Omega_i|}\sum_{j\in\mathcal{V}_{\text{int}}(i)} |\Gamma_{ij}| F\left(\mathbf{W}_i, \mathbf{W}_j, \mathbf{n}_{ij}\right) \\ + \frac{1}{|\Omega_i|}\sum_{j\in\mathcal{V}_{\text{wall}}(i)} |\Gamma_{ij}| F^{\text{wall}}\left(\mathbf{W}_i, \mathbf{n}_{ij}\right) \\ + \frac{1}{|\Omega_i|}\sum_{j\in\mathcal{V}_{\text{SW}}(i)} |\Gamma_{ij}| F^{\text{SW}}\left(\mathbf{W}_i, \mathbf{W}_b, \mathbf{n}_{ij}\right) = 0\end{aligned} \tag{16}$$

where the numerical flux F inside the domain, the Steger-Warming flux F^{SW} at inlet and outlet boundary conditions, and the flux at wall boundaries F^{wall} are defined in Appendix A.

We aim at performing an asymptotic expansion of the numerical scheme, and for this, we need to rephrase the numerical scheme (16) in term of the non-dimensional variables (4). We also consider

$$|\tilde{\Gamma}_{ij}| = \frac{|\Gamma_{ij}|}{x_0^{d-1}}, \quad |\tilde{\Omega}_i| = \frac{|\Omega_i|}{x_0^d}, \tag{17}$$

we get the dimensionless scheme

$$\begin{aligned}\partial_{\tilde{t}} \tilde{\mathbf{W}}_i + \frac{1}{|\tilde{\Omega}_i|}\sum_{j\in\mathcal{V}_{\text{int}}(i)} |\tilde{\Gamma}_{ij}| \tilde{F}\left(\tilde{\mathbf{W}}_i, \tilde{\mathbf{W}}_j, \mathbf{n}_{ij}, M\right) \\ + \frac{1}{|\tilde{\Omega}_i|}\sum_{j\in\mathcal{V}_{\text{wall}}(i)} |\tilde{\Gamma}_{ij}| \tilde{F}^{\text{wall}}\left(\tilde{\mathbf{W}}_i, \mathbf{n}_{ij}, M\right) \\ + \frac{1}{|\tilde{\Omega}_i|}\sum_{j\in\mathcal{V}_{\text{SW}}(i)} |\tilde{\Gamma}_{ij}| \tilde{F}^{\text{SW}}\left(\tilde{\mathbf{W}}_i, \tilde{\mathbf{W}}_b, \mathbf{n}_{ij}, M\right) = 0\end{aligned} \tag{18}$$

where the component associated to the variable w of the numerical flux and boundary flux are defined as

$$\tilde{F}_{\tilde{w}}\left(\tilde{\mathbf{W}}_i, \tilde{\mathbf{W}}_j, \mathbf{n}_{ij}, M\right) = \frac{1}{u_0 w_0} F_w\left(\mathbf{W}_0\tilde{\mathbf{W}}_i, \mathbf{W}_0\tilde{\mathbf{W}}_j, \mathbf{n}_{ij}\right)$$

where the products $\mathbf{W}_0\tilde{\mathbf{W}}_i$ should be understood componentwise. Details of the fluxes and boundary fluxes and their non-dimensional version are provided in Appendix A.

3.1.2 Formal asymptotic expansion of the schemes when the Mach number goes to 0

By doing the same formal two time-scales asymptotic development (7), but on the discrete system (18), we first prove the following result:

Proposition 3. *(Uniformity of $\tilde{\rho}^{(0)}$)*

- *If the numerical flux is conservative, namely*

$$F(W_i, W_j, \mathbf{n}_{ij}) = -F(W_j, W_i, \mathbf{n}_{ji}),$$

  and ensures

$$\tilde{F}_{\tilde{\rho}}\left(\tilde{\mathbf{W}}_i, \tilde{\mathbf{W}}_j, \mathbf{n}, M\right) = \frac{1}{M}\,\tilde{\alpha}\left(\tilde{\rho}_i^{(0)}, \tilde{\rho}_j^{(0)}\right)\left(\tilde{\rho}_i^{(0)} - \tilde{\rho}_j^{(0)}\right) + \mathcal{O}(1)$$

  where $\tilde{\alpha}\left(\tilde{\rho}_i^{(0)}, \tilde{\rho}_j^{(0)}\right)$ is strictly non-negative,

- *if the wall boundary flux ensures*

$$\tilde{F}_{\tilde{\rho}}^{wall}\left(\tilde{\mathbf{W}}_i, \mathbf{n}, M\right) = \mathcal{O}(1),$$

- *if the imposed boundary value $\tilde{\rho}_b^{(0)}$ on the Steger-Warming boundary conditions is constant,*
- *if the Steger-Warming flux ensures*

$$\tilde{F}_{\tilde{\rho}}^{SW}\left(\tilde{\mathbf{W}}_i, \mathbf{n}, M\right) = \frac{1}{M}\,\tilde{\beta}\left(\tilde{\rho}_i^{(0)}, \tilde{\rho}_b^{(0)}\right)\left(\tilde{\rho}_i^{(0)} - \tilde{\rho}_b^{(0)}\right) + \mathcal{O}(1)$$

  where $\tilde{\beta}\left(\tilde{\rho}_i^{(0)}, \tilde{\rho}_b^{(0)}\right)$ is strictly non-negative,

then

$$\forall i, \quad \tilde{\rho}_i^{(0)} = \tilde{\rho}_b^{(0)}.$$

Proof. As the flux of the density on the wall is always 0, the scale $\mathcal{O}\left(\frac{1}{M}\right)$ of the first equation of (18) gives, for all i:

$$\sum_{j\in\mathcal{V}_{\text{int}}(i)} |\tilde{\Gamma}_{ij}|\tilde{\alpha}\left(\tilde{\rho}_i^{(0)}, \tilde{\rho}_j^{(0)}\right)\left(\tilde{\rho}_i^{(0)} - \tilde{\rho}_j^{(0)}\right) + \sum_{j\in\mathcal{V}_{\text{SW}}(i)} |\tilde{\Gamma}_{ij}|\tilde{\beta}\left(\tilde{\rho}_i^{(0)}, \tilde{\rho}_b^{(0)}\right)\left(\tilde{\rho}_i^{(0)} - \tilde{\rho}_b^{(0)}\right) = 0$$

We multiply by $\tilde{\rho}_i^{(0)} - \tilde{\rho}_b^{(0)}$, and sum over all the cells of the mesh to find

$$\begin{aligned}\sum_{i\in\mathcal{T}_h}\sum_{j\in\mathcal{V}_{\text{int}}(i)} |\tilde{\Gamma}_{ij}|\left(\tilde{\rho}_i^{(0)} - \tilde{\rho}_b^{(0)}\right)\tilde{\alpha}\left(\tilde{\rho}_i^{(0)}, \tilde{\rho}_j^{(0)}\right)\left(\tilde{\rho}_i^{(0)} - \tilde{\rho}_j^{(0)}\right)\\ + \sum_{i\in\mathcal{T}_h}\sum_{j\in\mathcal{V}_{\text{SW}}(i)} |\tilde{\Gamma}_{ij}|\left(\tilde{\rho}_i^{(0)} - \tilde{\rho}_b^{(0)}\right)\tilde{\beta}\left(\tilde{\rho}_i^{(0)}, \tilde{\rho}_b^{(0)}\right)\left(\tilde{\rho}_i^{(0)} - \tilde{\rho}_b^{(0)}\right) = 0\end{aligned}$$

We switch to a sum over the faces of the mesh

$$\begin{aligned}\sum_{f\in\mathcal{F}_{\text{int}}} |\tilde{\Gamma}_f|\left(\left(\tilde{\rho}_L^{(0)} - \tilde{\rho}_b^{(0)}\right)\tilde{\alpha}\left(\tilde{\rho}_L^{(0)}, \tilde{\rho}_R^{(0)}\right)\left(\tilde{\rho}_L^{(0)} - \tilde{\rho}_R^{(0)}\right) + \left(\tilde{\rho}_R^{(0)} - \tilde{\rho}_b^{(0)}\right)\tilde{\alpha}\left(\tilde{\rho}_R^{(0)}, \tilde{\rho}_L^{(0)}\right)\left(\tilde{\rho}_R^{(0)} - \tilde{\rho}_L^{(0)}\right)\right)\\ + \sum_{f\in\mathcal{F}_{\text{SW}}} |\tilde{\Gamma}_f|\left(\tilde{\rho}_L^{(0)} - \tilde{\rho}_b^{(0)}\right)\tilde{\beta}\left(\tilde{\rho}_L^{(0)}, \tilde{\rho}_b^{(0)}\right)\left(\tilde{\rho}_L^{(0)} - \tilde{\rho}_b^{(0)}\right) = 0.\end{aligned}$$

As the scheme is conservative, we have

$$\tilde{\alpha}\left(\tilde{\rho}_L^{(0)}, \tilde{\rho}_R^{(0)}\right) = \tilde{\alpha}\left(\tilde{\rho}_R^{(0)}, \tilde{\rho}_L^{(0)}\right),$$

so that the sum may be rewritten

$$\begin{aligned}\sum_{f\in\mathcal{F}_{\text{int}}} |\tilde{\Gamma}_f|\tilde{\alpha}\left(\tilde{\rho}_L^{(0)}, \tilde{\rho}_R^{(0)}\right)\left(\tilde{\rho}_L^{(0)} - \tilde{\rho}_R^{(0)}\right)^2\\ + \sum_{f\in\mathcal{F}_{\text{SW}}} |\tilde{\Gamma}_f|\tilde{\beta}\left(\tilde{\rho}_L^{(0)}, \tilde{\rho}_b^{(0)}\right)\left(\tilde{\rho}_L^{(0)} - \tilde{\rho}_b^{(0)}\right)^2 = 0\end{aligned}$$

As the $\tilde{\alpha}$ and $\tilde{\beta}$ are strictly non-negative, we have on all interior faces $\tilde{\rho}_L^{(0)} = \tilde{\rho}_R^{(0)}$, which means that all the $\tilde{\rho}^{(0)}$ have the same value. Last, as all the $\tilde{\beta}$ are strictly non-negative, we have on all the Steger-Warming boundary faces $\tilde{\rho}_L^{(0)} = \tilde{\rho}_b^{(0)}$, so that if the set of Steger-Warming boundary sides is non empty, for all i, $\tilde{\rho}_i^{(0)} = \tilde{\rho}_b^{(0)}$, which ends the proof. □

We state now the link at the discrete level, between the discretization of (5) and (13). In general, a numerical scheme for (13) can be written as

$$\begin{aligned}
&\partial_\tau \mathbf{U}_i + \frac{1}{|\tilde{\Omega}_i|}\sum_{j\in\mathcal{V}_{\rm int}(i)} |\tilde{\Gamma}_{ij}| \left(A(\mathbf{n}_{ij}) \{\!\{ \mathbf{U} \}\!\}_{ij} - D(\mathbf{n}_{ij}) \left(\mathbf{U}_j - \mathbf{U}_i\right)\right) \\
&\quad + \frac{1}{|\tilde{\Omega}_i|}\sum_{j\in\mathcal{V}_{\rm wall}(i)} |\tilde{\Gamma}_{ij}| \left(A(\mathbf{n}_{ij}) \frac{\mathbf{U}_i}{2} + \frac{1}{2}\left(A(\mathbf{n}_{ij}) - 2A^-(\mathbf{n}_{ij}) P_{\rm wall}(\mathbf{n}_{ij})\right)\mathbf{U}_i\right) \\
&\quad + \frac{1}{|\tilde{\Omega}_i|}\sum_{j\in\mathcal{V}_{\rm SW}(i)} |\tilde{\Gamma}_{ij}| \left(A(\mathbf{n}_{ij}) \frac{\mathbf{U}_i + \mathbf{U}_b}{2} - \frac{1}{2}\left(A^+(\mathbf{n}_{ij}) - A^-(\mathbf{n}_{ij})\right)\left(\mathbf{U}_b - \mathbf{U}_i\right)\right) = 0,
\end{aligned} \tag{19}$$

where $\{\!\{ \mathbf{U} \}\!\}_{ij} = (\mathbf{U}_i + \mathbf{U}_j)/2$,

$$\mathbf{U} = \begin{pmatrix} \widehat{p} \\ \widehat{\mathbf{u}} \end{pmatrix}, \quad A(\mathbf{n}) = \begin{pmatrix} 0 & \frac{1}{\widehat{\rho_0}}\mathbf{n}^T \\ \widehat{\kappa_0}\mathbf{n} & 0 \end{pmatrix}, \quad P_{\rm wall}(\mathbf{n}) = \begin{pmatrix} 0 & 0 \\ 0 & 2\mathbf{n}\mathbf{n}^T \end{pmatrix},$$

and $D(\mathbf{n})$ depends on the numerical stabilization chosen. A^+ and A^- are the positive and negative parts of A. We can then prove the following consistency result with a discrete wave system:

Proposition 4 (Consistency with the wave system)**.** *We suppose that the hypotheses of Proposition 3 hold, so that $\tilde{\rho}_i^{(0)} = \tilde{\rho}_b^{(0)}$ for all i and we note*

$$\tilde{\alpha}_b^{(0)} := \tilde{\alpha}\left(\tilde{\rho}_b^{(0)}, \tilde{\rho}_b^{(0)}\right), \qquad \tilde{a}_b^{(0)} := \tilde{a}\left(\tilde{\rho}_b^{(0)}\right).$$

Moreover, we suppose that the numerical flux ensures the following asymptotic development (once $\tilde{\rho}_i^{(0)} = \tilde{\rho}_b^{(0)}$ is ensured)

$$\tilde{F}\left(\tilde{\mathbf{W}}_i, \tilde{\mathbf{W}}_j, \mathbf{n}, M\right) = \begin{pmatrix} \tilde{\rho}_b^{(0)} \dfrac{\left(\tilde{\mathbf{u}}_i^{(0)} + \tilde{\mathbf{u}}_j^{(0)}\right)\cdot\mathbf{n}}{2} + \tilde{\alpha}_b^{(0)}\left(\tilde{\rho}_i^{(1)} - \tilde{\rho}_j^{(1)}\right) + \mathcal{O}(M) \\ \dfrac{1}{M}\left(\dfrac{\left(\tilde{p}_i^{(1)} + \tilde{p}_j^{(1)}\right)\mathbf{n}}{2\gamma} + \mathbf{D}_{22}(\mathbf{n})\tilde{\rho}_b^{(0)}\left(\tilde{\mathbf{u}}_i^{(0)} - \tilde{\mathbf{u}}_j^{(0)}\right)\right) + \mathcal{O}(1) \end{pmatrix} \tag{20}$$

and that the boundary condition is well prepared as defined in (6), and that the boundary flux ensure the following asymptotic expansion

- *Wall boundary condition*

$$\tilde{F}^{wall}_{\tilde{\rho}\tilde{\mathbf{u}}}\left(\tilde{\mathbf{W}}_i, \mathbf{n}, M\right) = \frac{1}{M}\left(\frac{\tilde{p}_i^{(1)}}{\gamma}\mathbf{n} + \tilde{a}_b^{(0)}\tilde{\rho}_b^{(0)}\left(\tilde{\mathbf{u}}_i^{(0)}\cdot\mathbf{n}\right)\mathbf{n}\right) + \mathcal{O}(1) \tag{21}$$

- *Steger-Warming boundary condition*

$$\tilde{F}^{SW}\left(\tilde{\mathbf{W}}_i, \tilde{\mathbf{W}}_b, \mathbf{n}, M\right) = \begin{pmatrix} \tilde{\rho}_b^{(0)} \dfrac{\left(\tilde{\mathbf{u}}_i^{(0)} + \tilde{\mathbf{u}}_b^{(0)}\right)\cdot\mathbf{n}}{2} + \dfrac{\tilde{a}_b^{(0)}}{2}\left(\tilde{\rho}_i^{(1)} - \tilde{\rho}_b^{(1)}\right) + \mathcal{O}(M) \\ \dfrac{1}{M}\left(\left(\tilde{a}_b^{(0)}\right)^2 \dfrac{\tilde{\rho}_i^{(1)} + \tilde{\rho}_b^{(1)}}{2} + \dfrac{\tilde{a}_b^{(0)}\tilde{\rho}_b^{(0)}}{2}\left(\tilde{\mathbf{u}}_i^{(0)} - \tilde{\mathbf{u}}_b^{(0)}\right)\cdot\mathbf{n}\right)\mathbf{n} + \mathcal{O}(1) \end{pmatrix} \tag{22}$$

then $\left(\tilde{\rho}^{(1)}, (\tilde{\rho}\tilde{\mathbf{u}})^{(0)}\right)$ follows a discretization as (19) with $\widehat{\rho_0} = 1$, $\widehat{\kappa_0} = \left(\tilde{a}_b^{(0)}\right)^2$ ($\widehat{c_0} = \tilde{a}_b^{(0)}$), and with the numerical dissipation

$$D(\mathbf{n}) = \begin{pmatrix} \tilde{\alpha}_b^{(0)} & 0 \\ 0 & \mathbf{D}_{22}(\mathbf{n}) \end{pmatrix}.$$

Proof. We begin by reformulating the centered pressure of the second component of (20). The Mach expansion of the pressure can be written as

$$\tilde{p} = \tilde{p}^{(0)} + M\tilde{p}^{(1)} + \mathcal{O}\left(M^2\right),$$

but can be also obtained by using the equation of state and (10),

$$\begin{aligned}
\tilde{p} &= \tilde{p}(\tilde{\rho}) \\
&= \tilde{p}\left(\tilde{\rho}_b^{(0)} + M\tilde{\rho}^{(1)} + \mathcal{O}\left(M^2\right)\right) \\
&= \tilde{p}\left(\tilde{\rho}_b^{(0)}\right) + M\tilde{p}'\left(\tilde{\rho}_b^{(0)}\right)\tilde{\rho}^{(1)} + \mathcal{O}\left(M^2\right) \\
\tilde{p} &= \tilde{p}\left(\tilde{\rho}_b^{(0)}\right) + M\gamma\left(\tilde{a}_b^{(0)}\right)^2\tilde{\rho}^{(1)} + \mathcal{O}\left(M^2\right),
\end{aligned}$$

which leads to the equality

$$\tilde{p}^{(1)} = \gamma\left(\tilde{a}_b^{(0)}\right)^2\tilde{\rho}^{(1)}. \tag{23}$$

The discretization of (19) follows, by combining the $\mathcal{O}(1)$ and the $\mathcal{O}\left(\frac{1}{M}\right)$ of the numerical flux, and by using (23). □

With Proposition 4, it is possible to determine the asymptotic consistency of a given scheme for (1) with a discretization of the wave system (20). The hypothesis of Proposition 4 are checked for the boundary conditions in Appendix A. In this same section, it is also proven that

- if the Rusanov flux for the Euler system is used, then

$$\tilde{\alpha}_b^{(0)} = \frac{\tilde{a}_b^{(0)}}{2}, \qquad \mathbf{D}_{22}(\mathbf{n}) = \frac{\tilde{a}_b^{(0)}}{2}\mathrm{I}_d, \tag{24}$$

- if the Roe flux for the Euler system is used, then

$$\tilde{\alpha}_b^{(0)} = \frac{\tilde{a}_b^{(0)}}{2}, \qquad \mathbf{D}_{22}(\mathbf{n}) = \frac{\tilde{a}_b^{(0)}}{2}\mathbf{n}\mathbf{n}^T, \tag{25}$$

Note that the same asymptotic expansion can be performed on all the classical numerical fluxes. They are separated into two families:

- The ones that preserve the contact surface, for example: exact Godunov scheme, HLLC, HLLE, Osher. Theses solvers have an asymptotic expansion which gives (25).
- The ones that do not preserve the contact surface, for example, the HLL, or all the variants of the Rusanov scheme. Theses solvers have an asymptotic expansion which gives (24).

3.2 Schemes that are low Mach number accurate or not

As we did in the continuous case in subsection 2.1, we are now considering the limit of the discretization (19) of (11) when $\tau \to \infty$. We formally find

$$\begin{cases} \tilde{\rho}_h = \tilde{\rho}^{(0)} + M\hat{p}_h^{\infty} + \mathcal{O}\left(M^2\right) \\ \tilde{\rho}^{(0)}\tilde{u}_h = \hat{\mathbf{u}}_h^{\infty} + \mathcal{O}\left(M\right), \end{cases} \tag{26}$$

where $(\hat{p}_h^{\infty}, \hat{\mathbf{u}}_h^{\infty})$ is the long time limit of the matching discretization of the wave system provided by Proposition 4, with boundary conditions (12). The long time limit of symmetrizable linear systems was studied in [22]. More precisely, the existence of the long time limit was proved for stabilizations (24) and (25) and some features of the long time limit were studied numerically. Defining the discrete divergence on each cell K_i by

$$\left(\mathrm{div}_{\mathbf{x}}\mathbf{u}\right)_{K_i} = \frac{1}{|K_i|}\sum_{j\in\mathcal{V}(i)}\int_{\Gamma_{ij}} \{\!\{ \mathbf{u}\cdot\mathbf{n}_{ij} \}\!\}, \tag{27}$$

it was found that for the wave system

- On triangular meshes, with the stabilization (25), the long time limit is such that the pressure is 0, and the discrete divergence (27) is equal to 0. This result can be proved analytically. Indeed, in [18] (see also [33, 15]), it was proved that the limit is such that the jump of p and the jump of $\mathbf{u} \cdot \mathbf{n}$ are zero at all faces of the mesh. The discretely divergence-free velocity property follows. Since $p = 0$ on Steger-Warming boundary faces, the pressure is equal to 0.
- On non triangular meshes, with the stabilization (25), and with the stabilization (24) on any mesh, the long time limit is such that the pressure is nonzero.

Gathering these results on the linear wave system, with (26) leads to the well known result that

- On triangular meshes, the Roe scheme is low Mach number accurate whereas the Rusanov scheme is not.
- On quadrangular meshes, neither the Roe scheme nor the Rusanov scheme are low Mach number accurate.

Thus, for testing the non-accuracy at low Mach number of a nonlinear numerical flux for the barotropic Euler equations, we should first compute its low Mach number expansion, which leads to a stabilization of the wave system. Then the long time limit of this numerical discretization of the wave system is studied, and the numerical flux is not low Mach number accurate provided for a given test case (here, the scattering of a flow by a cylinder), this long time limit does not have a zero pressure or does not have a discretely divergence-free velocity. If the matching numerical discretization of the wave system has a zero pressure and a discretely divergence-free velocity on the same test case, then this is a hint for performing a more thorough study as it is done in the next section especially in Proposition 6.

4 A filtering method for steady low Mach number flows

In the previous section, we found that the low Mach number accuracy of a numerical flux could be studied by expanding this numerical flux in Mach number, and by studying the long time behavior of the matching discretization of the wave system.

In this section, we aim at going further: we want to use the numerical long time limit of the wave system for filtering the numerical solution of the Euler system. This will be led in three steps

1. Compute the steady solution $\mathbf{W}^{\text{Euler}}$ of the Euler system with the finite volume scheme (16), with boundary conditions ρ_b and $\mathbf{u}_b$ at the Steger-Warming boundary conditions.
2. Choose the density scale ρ_0 and the velocity scale u_0 in (4). Compute the long time limit of the matching wave system (11) in dimensionless variables with the matching finite volume scheme and initial condition, and with the boundary conditions $\widehat{p}_b = 0$ and $\widehat{u}_b = \left(\tilde{\rho}\tilde{\mathbf{u}}^{\text{Euler}}\right)_b^{(0)}$. We denote the discrete long time limit as $\widehat{p}_h^{\infty}$ and $\widehat{\mathbf{u}}_h^{\infty}$. From this, compute the numerical spurious component $\mathbf{W}^{\text{Spurious}}$ in dimensioned variables.
3. Subtract the spurious component from the Euler solution

$$\mathbf{W}^{\text{Filtered}} = \mathbf{W}^{\text{Euler}} - \mathbf{W}^{\text{Spurious}}$$

In the following subsections, we explain in details how $\mathbf{W}^{\text{Spurious}}$ is computed.

4.1 Filtered density

The following expansion holds in general when $M \to 0$

$$\tilde{\rho}_h^{\text{Euler}} = \left(\tilde{\rho}^{\text{Euler}}\right)_h^{(0)} + M\left(\tilde{\rho}^{\text{Euler}}\right)_h^{(1)} + \mathcal{O}\left(M^2\right).$$

The numerical scheme is low Mach number accurate only if $\left(\tilde{\rho}^{\text{Euler}}\right)_h^{(1)} = 0$. With (26), we know that the spurious component $\left(\tilde{\rho}^{\text{Euler}}\right)_h^{(1)}$ is the pressure $\widehat{p}_h^{\infty}$ of the long time limit of the matching wave system. The dimensionless filtered density is given by

$$\tilde{\rho}_h^{\text{Filtered}} = \tilde{\rho}_h^{\text{Euler}} - M\widehat{p}_h^{\infty},$$

so that the dimensioned filtered density is given by

$$\rho_h^{\text{Filtered}} = \rho_h^{\text{Euler}} - M\rho_0 \widehat{p}_h^{\infty}, \tag{28}$$

where $M = u_0/a_0$ and ρ_0, u_0 and a_0 correspond to the characteristic scales (4).

Then, we will get

$$\left(\tilde{\rho}^{\text{Filtered}}\right)_h^{(1)} = 0$$

as expected.

4.2 Filtered momentum

The computation of the filtered velocity is slightly more difficult than for the density: for the density, the full $\rho^{(1)}$ belongs to the spurious mode, whereas for the velocity, we know that $\mathbf{u}^{(0)}$ is not equal to 0. More precisely, the velocity of the long time solution of the wave system minus the divergence free component (in the sense of the decomposition (15)) of the initial condition of the wave system needs to be removed.

The filtering of the velocity can be deduced from a discrete version of Proposition 1, which exists only on triangles in 2D and on tetrahedra in 3D. We then extend this method to general finite element meshes. The method is described in 2D and the extension to 3D is specified.

4.2.1 Filtered momentum on triangular meshes

To simplify the notations, we denote $\mathcal{F}_{\text{wall/SW}}$ all the boundary faces

$$\mathcal{F}_{\text{wall/SW}} = \mathcal{F}_{\text{wall}} \cup \mathcal{F}_{\text{SW}}.$$

We define $\mathbf{u}_b$ on the wall boundary faces as $\mathbf{u}_b = 0$ such that the condition $\mathbf{u} \cdot \mathbf{n} = 0$ on walls can also be written as $\mathbf{u} \cdot \mathbf{n} = \mathbf{u}_b \cdot \mathbf{n}$.

In the triangular case, the following discrete equivalent of Proposition 1, is available:

Proposition 5 (Discrete Hodge-Helmholtz decomposition on triangular mesh)**.** *A piecewise constant velocity $\mathbf{u}_h$ on the triangular mesh $\mathcal{T}_h$ can be uniquely decomposed as*

$$\mathbf{u}_h = \mathcal{P}_h^{\varphi}\left[\mathbf{u}_h\right] + \mathcal{P}_h^{\mathbf{\Psi}}\left[\mathbf{u}_h\right]$$

where

- *$\mathcal{P}_h^{\varphi}\left[\mathbf{u}_h\right]$ and $\mathcal{P}_h^{\mathbf{\Psi}}\left[\mathbf{u}_h\right]$ are piecewise constant on the mesh $\mathcal{T}_h$,*
- *$\mathcal{P}_h^{\varphi}\left[\mathbf{u}_h\right]$ is the gradient of a Crouzeix-Raviart [9] scalar potential, i.e. $\mathcal{P}_h^{\varphi}\left[\mathbf{u}_h\right] = \nabla\varphi_h$ with*

$$\varphi_h \in W_h := \left\{\varphi_h \;\middle|\; \forall K \in \mathcal{T}_h,\ (\psi_h)_{|K} \in \mathbb{P}_1(K) \quad \text{and} \quad \varphi_h \text{ is continuous at the face midpoint}\right\},$$

- *$\mathcal{P}_h^{\mathbf{\Psi}}\left[\mathbf{u}_h\right] \in Z_h$ where*

$$Z_h := \left\{\mathbf{u}_h \in \mathbb{R}^{N_{\text{Cells}}^2} \;\middle|\; \forall f \in \mathcal{F}_{int},\ [\![\, \mathbf{u}_h \cdot \mathbf{n}_f \,]\!] = 0, \quad \forall f \in \mathcal{F}_{wall/SW},\ \mathbf{u}_i \cdot \mathbf{n}_f = \mathbf{u}_b \cdot \mathbf{n}_f\right\} \tag{29}$$

Moreover, we can prove that $\mathcal{P}_h^{\mathbf{\Psi}}\left[\mathbf{u}_h\right]$ is the curl of a continuous $\mathbb{P}_1$ potential vector, i.e. $\mathcal{P}_h^{\mathbf{\Psi}}\left[\mathbf{u}_h\right] = \nabla \times \psi_h$ with

$$\psi_h \in V_h := \left\{\psi_h \in C^0(\Omega) \;\middle|\; \forall K \in \mathcal{T}_h,\ (\psi_h)_{|K} \in \mathbb{P}_1(K)\right\}.$$

The proof of Proposition 5 is deferred to subsection B.3. It is an extension of [16, Theorem 4.1] in the H_0^1 case and of [15, Lemma 3.1] or [13, Lemme 3.5] in the periodic case.

The decomposition of Proposition 5 is adapted to the discretization of the wave system with the stabilization (25), as it was previously explained in [15] in the periodic case. More precisely, we have the following proposition which is a discrete version of Proposition 2

Proposition 6. *If we use the discrete wave system (19) on a triangular mesh with the stabilization (25) and with a forward Euler method for time integration, a state $(\widehat{p}_h^0, \widehat{\mathbf{u}}_h^0)$ such that $\widehat{p}_h^0$ is uniform (equals to $\widehat{p}_b$) and $\mathcal{P}_h^{\varphi}\left[\widehat{\mathbf{u}}_h^0\right] = 0$ is constant in time.*

The proof is deferred to subsection B.4.

Suppose now that we are dealing with the Rusanov scheme, which matches the stabilization (24) of the wave system. Then the Proposition 6 does not hold for this stabilization; moreover, the discrete divergence (27) of the long time limit of the velocity is not 0. Nevertheless, the initial condition of the wave system $\hat{\mathbf{u}}_h^0$ can be decomposed as

$$\hat{\mathbf{u}}_h^0 = \mathcal{P}_h^{\varphi}\left[\hat{\mathbf{u}}_h^0\right] + \mathcal{P}_h^{\mathbf{\Psi}}\left[\hat{\mathbf{u}}_h^0\right].$$

Then the spurious component of the velocity clearly appears as being $\hat{\mathbf{u}}_h^{\infty} - \mathcal{P}_h^{\mathbf{\Psi}}\left[\hat{\mathbf{u}}_h^0\right]$. Based on the proof of Proposition 5 detailed in subsection B.3, the component $\mathcal{P}_h^{\varphi}\left[\hat{\mathbf{u}}_h^0\right]$ can be computed by solving the variational problem

$$\text{Find } \varphi_h \in W_h \quad \forall g_h \in W_h \qquad \sum_K \int_K \nabla_{\mathbf{x}} g_h \cdot \nabla_{\mathbf{x}} \varphi_h = \sum_K \int_K \hat{\mathbf{u}}_h^0 \cdot \nabla g_h - \sum_{f \in \mathcal{F}_{\text{wall/SW}}} \int_f g_h \hat{\mathbf{u}}_b \cdot \mathbf{n} \tag{30}$$

and by computing the cell-by-cell gradient of φ_h. $\mathcal{P}_h^{\mathbf{\Psi}}\left[\hat{\mathbf{u}}_h^0\right]$ is then computed as $\mathcal{P}_h^{\mathbf{\Psi}}\left[\hat{\mathbf{u}}_h^0\right] = \hat{\mathbf{u}}_h^0 - \mathcal{P}_h^{\varphi}\left[\hat{\mathbf{u}}_h^0\right]$. This leads to the following filtered momentum

$$(\rho\mathbf{u})^{\text{Filtered}} = (\rho\mathbf{u})^{\text{Euler}} - \rho_0 u_0 \left(\hat{\mathbf{u}}_h^{\infty} - \mathcal{P}_h^{\mathbf{\Psi}}\left[\hat{\mathbf{u}}_h^0\right]\right). \tag{31}$$

4.2.2 Filtered momentum on quadrangular meshes

We have no knowledge of a decomposition similar to Proposition 5 on quadrangular meshes. It is of course possible to use a formulation similar to (30) by replacing the Crouzeix-Raviart finite element space by its equivalent for nonconforming finite elements approximations on quad meshes: the Rannacher-Turek finite element space [30]. However contrary to triangles in which the cell-by-cell derivative of a Crouzeix-Raviart function belongs to $\mathbb{P}_0$, the cell-by-cell derivative of a Rannacher-Turek function is not in $\mathbb{Q}_0$. As a consequence a $\mathcal{P}_h^{\varphi}\left[\hat{\mathbf{u}}_h^0\right]$ belonging to $\mathbb{Q}_0$ cannot be defined as the cell-by-cell gradient of φ_h. Instead, we define $\overline{\mathcal{P}_h^{\varphi}\left[\hat{\mathbf{u}}_h^0\right]}$ as a $\mathbb{Q}_0$ approximation on each cell: the average of the gradient of φ_h on each cell:

$$\forall K \in \mathcal{T}_h \qquad \overline{\mathcal{P}_h^{\varphi}\left[\hat{\mathbf{u}}_h^0\right]}_K = \frac{1}{|K|}\int_K \nabla_{\mathbf{x}} \varphi_h. \tag{32}$$

Note that on triangles, $\overline{\mathcal{P}_h^{\varphi}\left[\hat{\mathbf{u}}_h^0\right]} = \mathcal{P}_h^{\varphi}\left[\hat{\mathbf{u}}_h^0\right]$. The filtered momentum on quadrangular meshes is then defined as (31), by using $\overline{\mathcal{P}_h^{\varphi}\left[\hat{\mathbf{u}}_h^0\right]}$ instead of $\mathcal{P}_h^{\varphi}\left[\hat{\mathbf{u}}_h^0\right]$:

$$(\rho\mathbf{u})^{\text{Filtered}} = (\rho\mathbf{u})^{\text{Euler}} - \rho_0 u_0 \left(\hat{\mathbf{u}}_h^{\infty} - \overline{\mathcal{P}_h^{\mathbf{\Psi}}\left[\hat{\mathbf{u}}_h^0\right]}\right), \tag{33}$$

where $\overline{\mathcal{P}_h^{\mathbf{\Psi}}\left[\hat{\mathbf{u}}_h^0\right]} := \hat{\mathbf{u}}_h^0 - \overline{\mathcal{P}_h^{\varphi}\left[\hat{\mathbf{u}}_h^0\right]}$.

4.3 Summary of the filtering method

For a given mesh and a given distribution of the Steger-Warming and wall boundary conditions

1. Determine the wave stabilization matching the numerical flux used.
2. Compute the long time limit $\hat{p}_h^{\infty}$ and $\hat{\mathbf{u}}_h^{\infty}$ of the wave system, with $\hat{p}_b = 0$ and $\hat{\mathbf{u}}_b = (\tilde{\rho}\tilde{\mathbf{u}}^{\text{Euler}})_b^{(0)}$ on the Steger-Warming boundary conditions.
3. Compute $\overline{\mathcal{P}_h^{\varphi}\left[\hat{\mathbf{u}}_h^0\right]}$ by solving (30) and by using then (32). From a practical point of view, (30) is solved by using PETSc with the conjugate gradient method. Note that because of the Neumann boundary conditions, the variational formulation (30) has a kernel matching uniform potentials, so that direct methods are not well suited.
4. Filter the solution by using (28) and (33).

Since dimensionless variables are used, it is important to note that all the computations needed for the filtering phase are independent of the Mach number. Also, all these computations are linear.

The filtering method naturally extends to 3D. Of course, we have to compute the numerical long time solution $(\hat{p}_h^{\infty}, \hat{\mathbf{u}}_h^{\infty})$ of the matching wave system in 3D. The filtered density is obtained with (28) as in 2D. For the filtered momentum, we also use (33) where $\mathcal{P}_h^{\varphi}\left[\hat{\mathbf{u}}_h^0\right]$ is obtained by solving the variational problem (30) with Crouzeix-Raviart finite element space on tetrahedral mesh or with Rannacher-Turek finite element space on hexahedral mesh.

5 Numerical results

In this section, we test the filtering method described in the previous section to compute low Mach number steady solution of the Euler equations (1) with the finite volume scheme (16).

5.1 Test case description

We consider an open domain Ω with a number of obstacles Ω_l, such that the boundaries of Ω and Ω_l are regular. Boundary conditions set on $\partial\Omega_l$ are of wall type, whereas on $\partial\Omega$, Steger-Warming boundary conditions are imposed with a state characterized by its density at infinity ρ_b, and its Mach number at infinity M_b. All the computations are led with the equation of state

$$p(\rho) = \rho^2.$$

For all the computations, an external density of $\rho_b = 2$ is imposed, and the external velocity is deduced from the Mach number by $\mathbf{u}_b = (M_b\sqrt{p'(\rho_b)}, 0)^T$. The initial data are uniform and set equal to

$$\rho = \rho_b, \qquad \mathbf{u} = \mathbf{0}.$$

All simulations were run with a forward Euler time stepping with a CFL number of 0.4.

5.2 Matching wave system

To apply the filtering method, we need to compute the long time limit of a wave problem. Choosing $\rho_0 = \rho_b$ for the density scale and $u_0 = M_b\sqrt{p'(\rho_b)}$ for the velocity scale, the matching wave problem (13) is obtained with $\widehat{\rho_0} = \widehat{\kappa_0} = 1$ and the matching finite volume scheme is (19) where at the Steger-Warming boundary condition we have $\widehat{p}_b = 0$ and $\widehat{\mathbf{u}}_b = (1, 0)^T$.

5.3 Flow around a Cylinder

In this section, we are interested in the case when a single cylinder obstacle is in Ω. This test case is interesting because an exact solution of the velocity field $\mathbf{u}^{(0)}$ is known in the low Mach number limit provided the computational domain is a ring between the cylinder, which radius is r_0 and the external part of the computational domain, which is of radius r_1:

$$\mathbf{u}^{(0)}_{\text{ex}} = M_b\sqrt{p'(\rho_b)}\frac{r_1^2}{r_1^2 - r_0^2}\begin{pmatrix} 1 - \dfrac{r_0^2}{r^2}\cos(2\theta) \\ -\dfrac{r_0^2}{r^2}\sin(2\theta) \end{pmatrix}. \tag{34}$$

The numerical results are obtained with $r_0 = 0.5$ and $r_1 = 5.5$. For all the studies except for the one with mesh convergence, the test is performed on a triangular and a quadrangular mesh with the following characteristics. The quadrangular mesh is obtained by discretizing the annulus $[r_0, r_1] \times [0, 2\pi[$ with a resolution of $n_r = 50$ in the radial direction and $n_\theta = 160$ in the orthoradial direction. This mesh contains 8 000 quadrangular cells. The triangular mesh is obtained from a quadrangular mesh produced with $n_r = 25$ and $n_\theta = 80$ by dividing each quadrangle into two triangles. This mesh contains 4 000 triangular cells.

We first aim at illustrating the convergence towards a steady state for the Euler system. In Figure 1, the density residual

$$\max_i \left| |\Omega_i| \frac{\rho_i^{n+1} - \rho_i^n}{\delta t} \right|$$

and the momentum residuals are plotted as a function of the time. Even if the time required depends on the Mach number, the mesh and the numerical scheme, all schemes allow to reach a steady state. For similar results on the matching wave system, we refer to [22]. All the results presented in the following match a final computational time for which all the residuals are converged. This final time depends on the mesh, the Mach number and the scheme used.

In Figure 2, the L^2 norm of density fluctuation $\rho - \rho_b$ is plotted with respect to the Mach number (for $M_b = 10^{-1}$ to $M_b = 10^{-10}$) on quadrangular (8 000 cells) and triangular (4 000 cells) mesh. Results with and without filtering are shown. Without filtering, as expected, a $\mathcal{O}(M)$ scaling of the density fluctuation is obtained for the Rusanov and Roe schemes on the quadrangular mesh [19], and for the Rusanov scheme on the triangular mesh [31]. A $\mathcal{O}(M^2)$ scaling is obtained for the Roe scheme on the triangular mesh [33, 18]. With filtering, all the numerical solutions recover the $\mathcal{O}(M^2)$ behavior. For some schemes, the convergence rate is lost for Mach number smaller

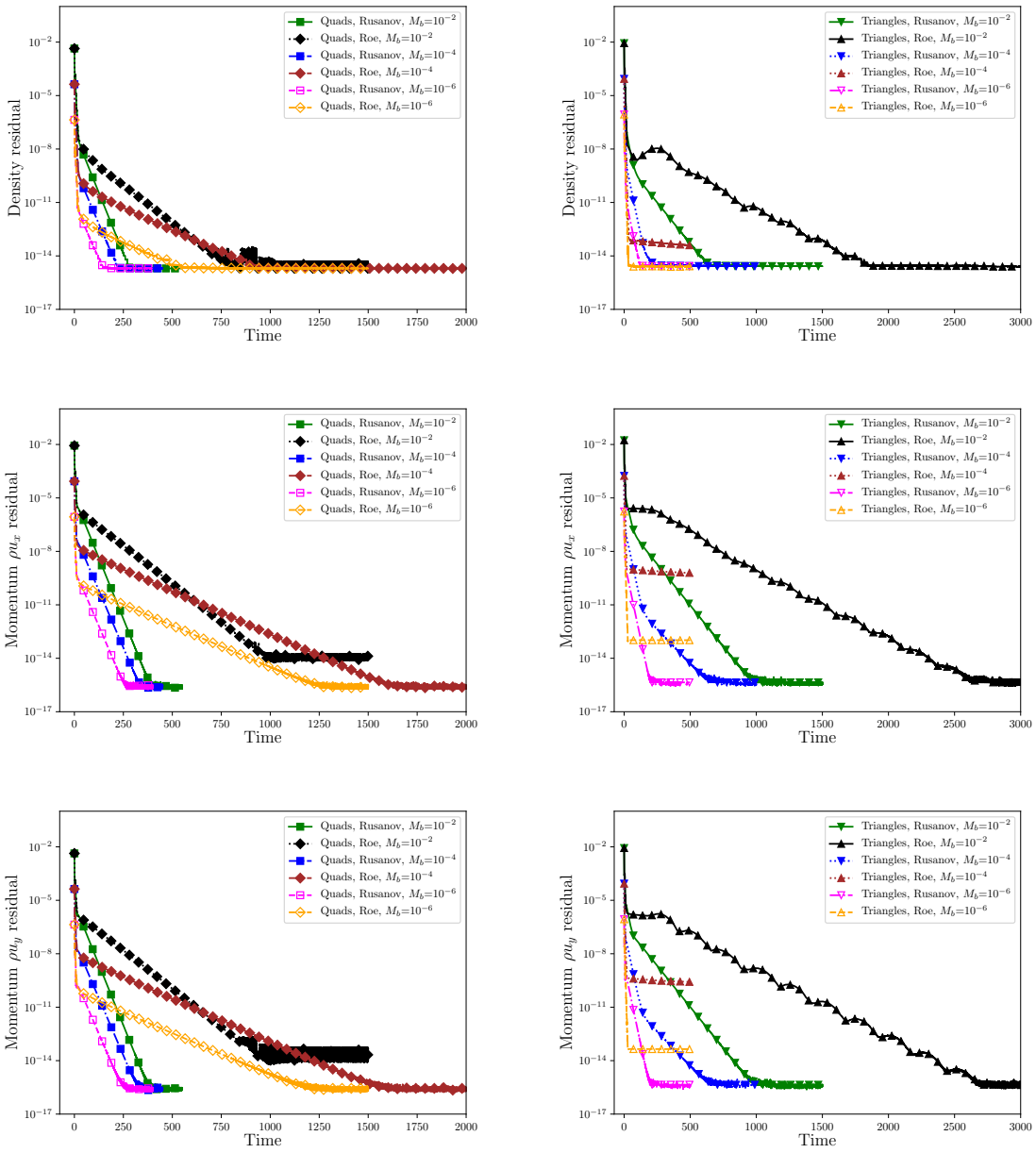

Figure 1: Residual obtained with quadrangular and triangular mesh on the density and the momentum ρu_x and ρu_y as a function of the time.

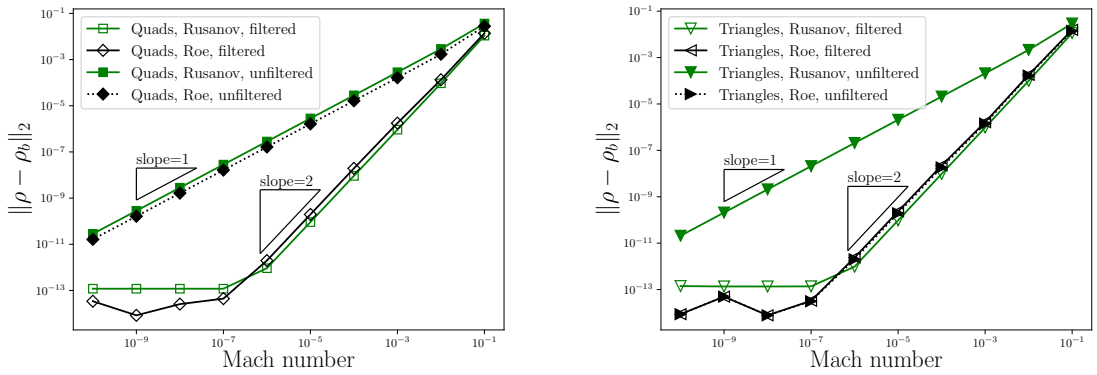

Figure 2: L^2 norm of density fluctuation $\rho - \rho_b$ with respect to the Mach number (for $M_b = 10^{-1}$ to $M_b = 10^{-10}$). Rusanov and Roe schemes are used on triangular (right) and quadrangular (left) mesh. A log-log plot is used. Results with and without filtering are shown, and confirm that filtering allows to recover the $\mathcal{O}\left(M^2\right)$ scaling of the density fluctuation (or pressure fluctuation) when the Mach number goes to 0.

than 10^{-7} because the numerical precision limit is reached. These results validate the link between the long time pressure of the wave system and the spurious mode in the low Mach number limit that was proposed in the filtering of the density in (28).

In Figure 3 and Figure 4, the iso-contours of the norm of the velocity obtained at $M_b = 10^{-4}$ are plotted. Results with and without filtering are shown on triangular and quadrangular mesh and are compared to the reference solution (34). Results show that even if the unfiltered solution is very far from the reference solution, the filtering method allows to recover a solution close to the reference solution. These results validate the filtering of the momentum that was proposed in (33).

In Figure 5, a grid convergence study on the velocity field is performed on triangular and quadrangular meshes. Rusanov and Roe scheme are used with and without filtering. Four different meshes are used in both cases. Without filtering, the Rusanov scheme on triangular and quadrangular mesh and the Roe scheme on quadrangular mesh do not converge to the reference solution. However, the Roe scheme on triangular mesh converges to the reference solution with a rate of 1. With filtering, the convergence with a rate of 1 on quadrangular and triangular mesh is recovered for the Rusanov and the Roe scheme. These results confirm the relevance of the filtering of the momentum of (33).

5.4 Flow around a NACA0012 airfoil

In this section, the filtering method is tested on a low Mach number flow around a NACA0012 included in a rectangular domain $[-1; 2] \times [-2; 2]$. Two meshes are used:

- a triangular mesh generated with `GMSH`[17] with a characteristic length $lc = 0.024$ around the NACA profile, and $5lc$ on the external boundaries.
- an unstructured quadrangular mesh, still generated with `GMSH` by recombination of a triangular mesh on which the blossom algorithm is applied.

For this computation, no exact solution is known. However, we still expect the density fluctuations around ρ_b to scale as $\mathcal{O}\left(M^2\right)$ when the Mach number goes to 0. Results obtained for this scaling are shown on Figure 6. They confirm that without filtering, a $\mathcal{O}\left(M\right)$ scaling is obtained for the Rusanov and Roe scheme on the quadrangular mesh, and for the Rusanov scheme on the triangular mesh. Once filtered, all the numerical solutions recover a $\mathcal{O}\left(M^2\right)$ behavior. Last, a well known result is observed: the Roe scheme on the triangular mesh has a $\mathcal{O}\left(M^2\right)$ behavior without any filtering. We are now interested in the results of the velocity. In this case, the numerical solution obtained with the Roe scheme on triangles is taken as a reference solution. Results obtained for a Mach number $M_b = 10^{-4}$ are shown in Figure 7. Results prove that the filtering method developed in this article allows to recover a good solution, even with the solution with the very noised solution obtained with the Roe scheme on quadrangular meshes (We believe that the very noisy solution

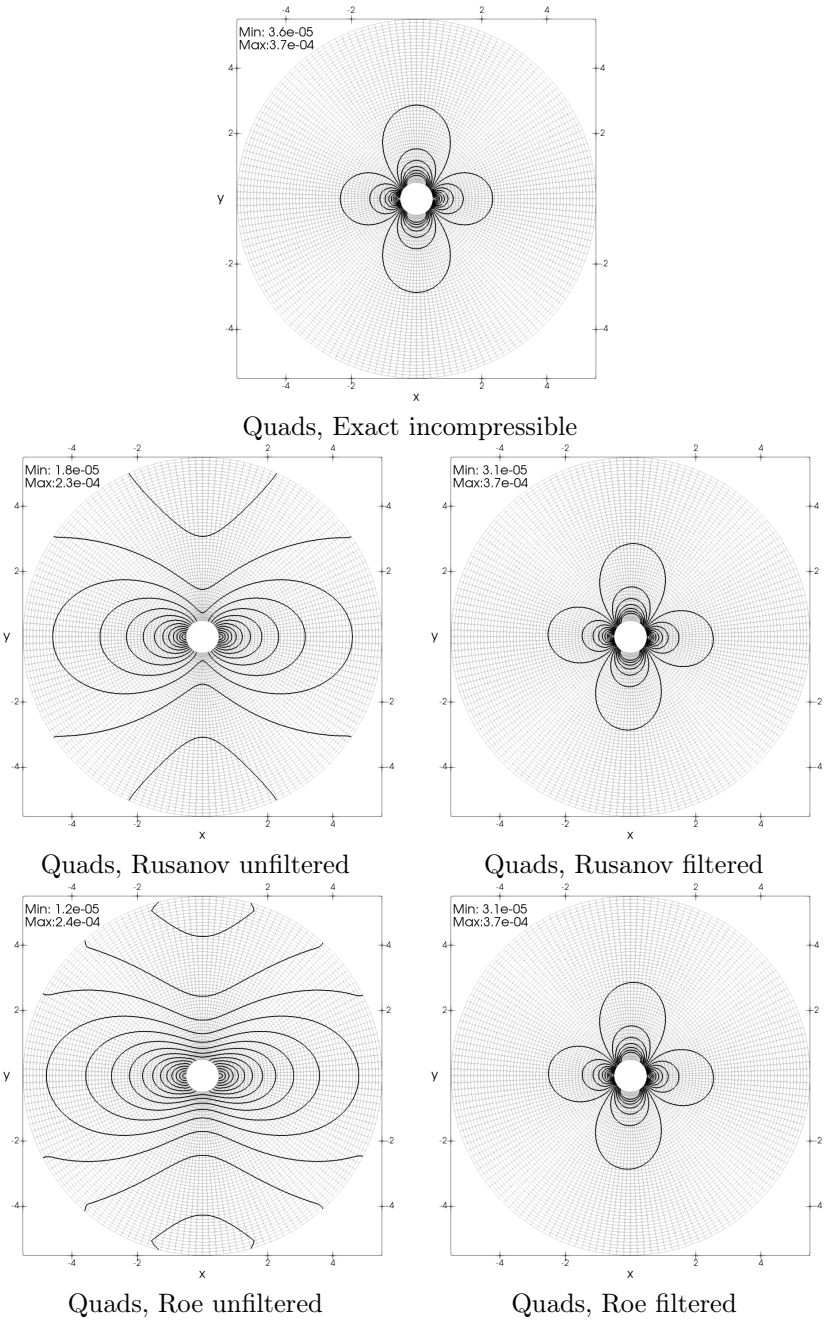

Figure 3: Iso-contours of the norm of the velocity obtained at Mach number $M_b = 10^{-4}$ on quadrangular mesh. Results with and without filtering are shown for the Rusanov and the Godunov scheme. Twenty equally reparted contours between 8×10^{-6} and 3×10^{-4} are plotted.

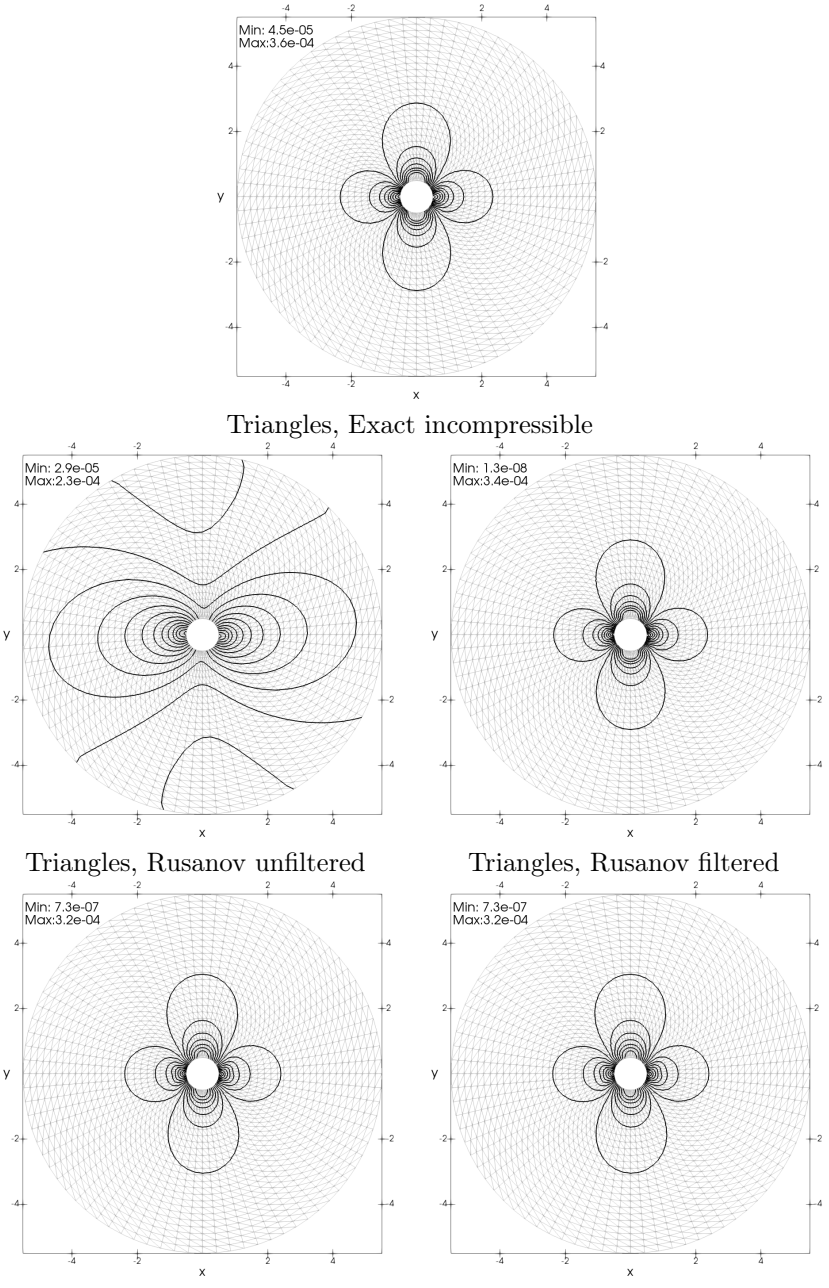

Figure 4: Iso-contours of the norm the velocity obtained at Mach number $M_b = 10^{-4}$ on triangular mesh. Results with and without filtering are shown for the Rusanov and the Godunov scheme. Twenty equally reparted contours between 8×10^{-6} and 3×10^{-4} are plotted.

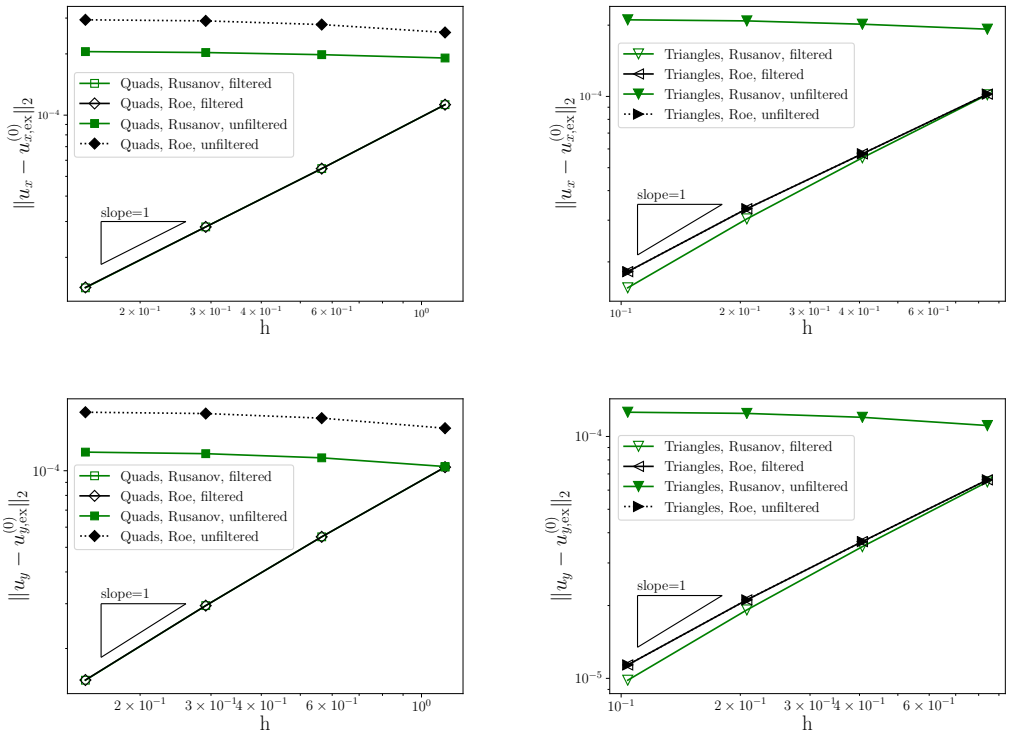

Figure 5: L_2 norm of the velocity error between the exact incompressible solution and the long time limit state obtained with the Rusanov and the Godunov scheme. Results with and without filtering are shown on quadrangular (left) and triangular (right) meshes for a Mach number of $M_b = 10^{-4}$.

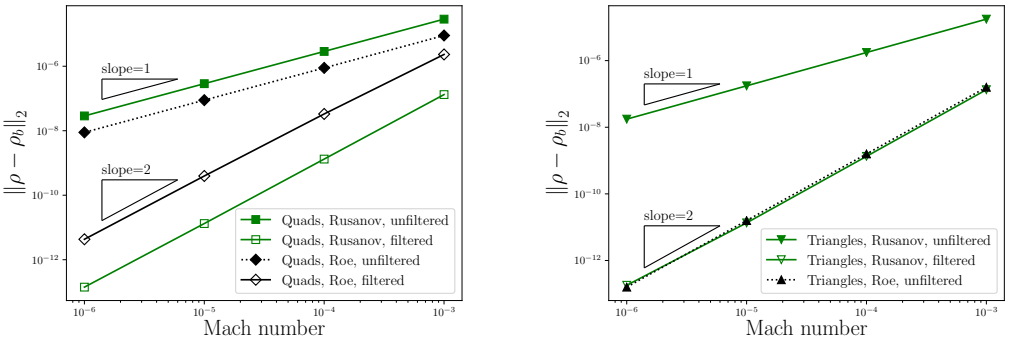

Figure 6: Results obtained for the L^2 norm of $\|\rho - \rho_b\|$ with respect to the Mach number. A log-log plot is used. Rusanov and Roe scheme are used on both triangular (right) and quadrangular (left) meshes, and results with and without filtering are shown, and confirm that filtering allows to recover the M^2 scaling for the density when the Mach number goes to 0.

with the Roe solver is induced by the use of a quad mesh obtained with the blossom algorithm, which is strongly different to the O-meshes used usually for NACA computations).

6 Conclusion

In this article, the behavior of numerical schemes for compressible flows in the low Mach number limit was enlightened to share a lot of properties with the long time behavior of the discretization of a wave system. We deduce that the numerical fluxes for (1) can be divided into two families:

- The numerical fluxes that are low Mach number accurate, which are matching a discretization of the wave system for which the long time limit ensures a uniform pressure and an irrotational velocity for all configurations defined by equations (13),(14).
- The numerical fluxes that are not low Mach accurate, which are matching a discretization of the wave system for which the long time limit does not ensure a uniform pressure nor an irrotational velocity for at least one configuration defined by equations (13),(14).

This means that for studying the low Mach number accuracy of a numerical scheme for (1), it is sufficient to study the long time limit of a matching discretization of the wave system, which is much easier because it is a linear problem.

In the triangular case, a sharp algebraic framework including a discrete Hodge-Helmholtz decomposition with initial condition and boundary conditions allowed to extend the accuracy on triangles for some numerical fluxes. This result was already known in the unbounded case [15, 18].

In the case of a numerical flux not accurate at low Mach number, the spurious mode was identified (up to a factor) as

- For the pressure, the pressure component of the long-time limit of the wave system.
- For the velocity, the long time limit of the wave system minus the divergence free component (as defined in Proposition 1) of the initial velocity of the wave system.

From the exact knowledge of the spurious mode, a filtering method was proposed. We proved that with this method, an accuracy comparable with numerical fluxes accurate at low Mach number could be recovered. This filtering needs only the long time limit of the wave system for the filtering of the pressure, and needs also the inversion of one Laplace system for the computation of the divergence free component of the initial velocity.

This article deals only with finite volume schemes, however, we would like to stress that our methodology is very generic: all the results obtained can be applied in any numerical scheme, especially the asymptotic expansion of the numerical scheme for checking compatibility with the wave system (section 2), and Hodge-Helmholtz decomposition for filtering the steady low Mach number solution (section 4).

We consider the identification of the spurious mode at low Mach number as an important step for deriving accurate low Mach number numerical methods. We were able here to use this spurious mode for developing a filtering method but only for stationary barotropic Euler computations. There is still a lot of work for extending this method to full Euler system, to unstationary problems, or to viscous problems. As far as the full Euler system is concerned, the difficulty would be raised by the fact that the pressure is constant, but other thermodynamic variables (temperature, density) are not, so that the sound velocity of the matching wave system would not be uniform within the computational domain. The result of [22] would still hold, as uniformity of the wave velocity is not required. Last, the Hodge-Helmholtz decomposition of Proposition 5 would probably need to be modified, for example by being weighted by the sound velocity field as in [13].
For the extension towards time dependent or viscous flows, we are currently trying to develop a reformulation of the system as a fluctuation around the spurious mode. This is a strategy that is usually developed for getting well balanced schemes for hyperbolic systems with a source term, by formulating the system as a fluctuation around the steady state [6].

Acknowledgment: Experiments presented in this article were carried out using the PlaFRIM experimental testbed, supported by Inria, CNRS (LABRI and IMB), Université de Bordeaux, Bordeaux INP and Conseil Régional d'Aquitaine (see https://www.plafrim.fr/).

References

[1] W. Barsukow. Stationarity preserving schemes for multi-dimensional linear systems. *Mathematics of Computation*, 88(318):1621–1645, 2019.

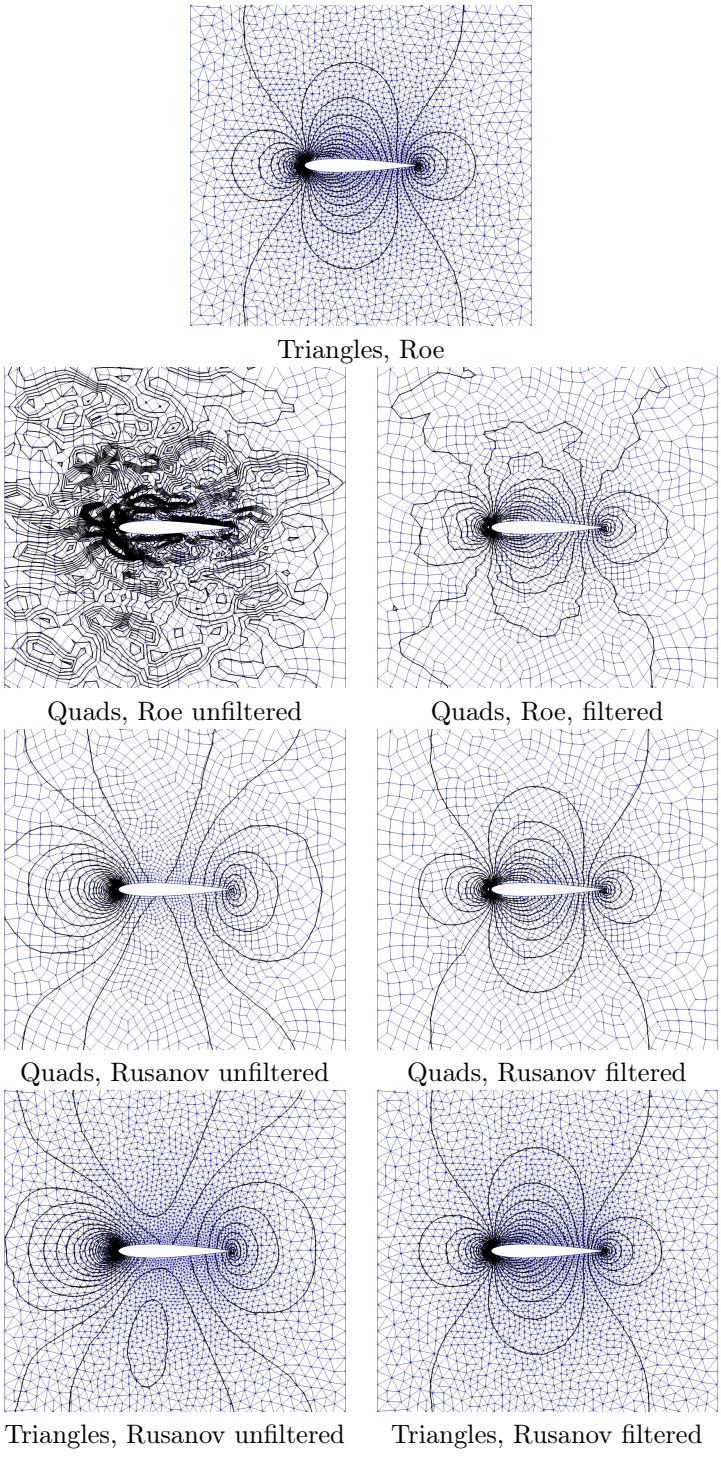

Figure 7: Iso-contours of the velocity obtained for the different schemes, meshes, and with or without filtering. Fifty equally reparted contours of the norm of the velocity between $9.51125e-05$ and 0.000235117 are plotted. The solution obtained with the Roe scheme on triangles is taken as a reference.

[2] W. Barsukow. Truly multi-dimensional all-speed schemes for the Euler equations on Cartesian grids. *Journal of Computational Physics*, 435:110216, 2021.

[3] W. Boscheri, G. Dimarco, R. Loubère, M. Tavelli, and M.-H. Vignal. A second order all Mach number IMEX finite volume solver for the three dimensional Euler equations. *Journal of Computational Physics*, 415:109486, 2020.

[4] F. Bouchut, E. Franck, and L. Navoret. A low cost semi-implicit low-Mach relaxation scheme for the full Euler equations. *Journal of Scientific Computing*, 83(1):1–47, 2020.

[5] P. Bruel, S. Delmas, J. Jung, and V. Perrier. A low Mach correction able to deal with low Mach acoustics. *Journal of Computational Physics*, 378:723–759, 2019.

[6] M. Castro, J. M. Gallardo, J. A. López-GarcÍa, and C. Parés. Well-balanced high order extensions of Godunov's method for semilinear balance laws. *SIAM Journal on Numerical Analysis*, 46(2):1012–1039, 2008.

[7] C. Chalons, M. Girardin, and S. Kokh. An all-regime Lagrange-Projection like scheme for the gas dynamics equations on unstructured meshes. *Communications in Computational Physics*, 20(1):188–233, 2016.

[8] F. Cordier, P. Degond, and A. Kumbaro. An asymptotic-preserving all-speed scheme for the Euler and Navier–Stokes equations. *Journal of Computational Physics*, 231(17):5685–5704, 2012.

[9] M. Crouzeix and P.-A. Raviart. Conforming and nonconforming finite element methods for solving the stationary Stokes equations I. *ESAIM: Mathematical Modelling and Numerical Analysis-Modélisation Mathématique et Analyse Numérique*, 7(R3):33–75, 1973.

[10] P. Degond, S. Jin, and J. Yuming. Mach-number uniform asymptotic-preserving gauge schemes for compressible flows. *Bulletin-Institute of Mathematics Academia Sinica*, 2(4):851, 2007.

[11] P. Degond and M. Tang. All speed scheme for the low Mach number limit of the isentropic Euler equations. *Communications in Computational Physics*, 10(1):1–31, 2011.

[12] S. Dellacherie. Analysis of Godunov type schemes applied to the compressible Euler system at low Mach number. *Journal of Computational Physics*, 4(229):978–1016, 2010.

[13] S. Dellacherie, J. Jung, and P. Omnes. Construction of a low Mach finite volume scheme for the isentropic Euler system with porosity. *ESAIM: Mathematical Modelling and Numerical Analysis*, 55(3):1199–1237, 2021.

[14] S. Dellacherie, J. Jung, P. Omnes, and P.-A. Raviart. Construction of modified Godunov type schemes accurate at any Mach number for the compressible Euler system. *Mathematical Models and Methods in Applied Sciences*, Nov. 2016.

[15] S. Dellacherie, P. Omnes, and F. Rieper. The influence of cell geometry on the Godunov scheme applied to the linear wave equation. *Journal of Computational Physics*, 229(14):5315–5338, 2010.

[16] A. Douglas N. and F. Richard S. A uniformly accurate finite element method for the Reissner–Mindlin plate. *SIAM J. Numer. Anal.*, 26:1276–1290, 1989.

[17] C. Geuzaine and J.-F. Remacle. Gmsh: A 3-d finite element mesh generator with built-in pre-and post-processing facilities. *International journal for numerical methods in engineering*, 79(11):1309–1331, 2009.

[18] H. Guillard. On the behavior of upwind schemes in the low Mach number limit. IV: P0 approximation on triangular and tetrahedral cells. *Computers & Fluids*, 38(10):1969–1972, 2009.

[19] H. Guillard and C. Viozat. On the behaviour of upwind schemes in the low Mach number limit. *Computers & fluids*, 28(1):63–86, 1999.

[20] J. Haack, S. Jin, and J.-G. Liu. An all-speed asymptotic-preserving method for the isentropic Euler and Navier-Stokes equations. *Communications in Computational Physics*, 12(4):955–980, 2012.

[21] D. Iampietro, F. Daude, P. Galon, and J.-M. Hérard. A Mach-Sensitive Splitting Approach for Euler-like Systems. *ESAIM: Mathematical Modelling and Numerical Analysis*, 2018.

[22] J. Jung and V. Perrier. Long time behavior of finite volume discretization of symmetrizable linear hyperbolic systems. *IMA Journal of Numerical Analysis*, 2021.

[23] K. Kaiser, J. Schütz, R. Schöbel, and S. Noelle. A new stable splitting for the isentropic Euler equations. *Journal of scientific computing*, 70(3):1390–1407, 2017.

[24] S. Klainerman and A. Majda. Singular limits of quasilinear hyperbolic systems with large parameters and the incompressible limit of compressible fluids. *Communications on pure and applied Mathematics*, 34(4):481–524, 1981.

[25] X.-s. Li and C.-w. Gu. An all-speed Roe-type scheme and its asymptotic analysis of low Mach number behaviour. *Journal of Computational Physics*, 227(10):5144–5159, 2008.

[26] X.-s. Li, C.-w. Gu, and J.-z. Xu. Development of Roe-type scheme for all-speed flows based on preconditioning method. *Computers & Fluids*, 38(4):810–817, 2009.

[27] B. Müller. Low Mach number asymptotics of the Navier-Stokes equations and numerical implications. In *VKI Lecture Series on Computational fluid dynamics*, pages 1–52, 1999.

[28] R. A. Nicolaides. Direct discretization of planar div-curl problems. *SIAM Journal on Numerical Analysis*, 29(1):32–56, 1992.

[29] K. Oß wald, A. Siegmund, P. Birken, V. Hannemann, and A. Meister. L^{2}Roe: a low dissipation version of Roe's approximate Riemann solver for low Mach numbers. *Internat. J. Numer. Methods Fluids*, 81(2):71–86, 2016.

[30] R. Rannacher and S. Turek. Simple nonconforming quadrilateral Stokes element. *Numerical Methods for Partial Differential Equations*, 8(2):97–111, 1992.

[31] F. Rieper. On the dissipation mechanism of upwind-schemes in the low Mach number regime: A comparison between Roe and HLL. *Journal of Computational Physics*, 229(2):221–232, 2010.

[32] F. Rieper. A low-Mach number fix for Roe's approximate Riemann solver. *Journal of Computational Physics*, 230(13):5263–5287, 2011.

[33] F. Rieper and G. Bader. The influence of cell geometry on the accuracy of upwind schemes in the low Mach number regime. *Journal of Computational Physics*, 228(8):2918–2933, 2009.

[34] S. Schochet. Fast singular limits of hyperbolic PDEs. *Journal of differential equations*, 114(2):476–512, 1994.

[35] E. Turkel. Preconditioned methods for solving the incompressible and low speed compressible equations. *Journal of Computational Physics*, 72(2):277–298, 1987.

[36] E. Turkel and V. Vatsa. Local preconditioners for steady state and dual time-stepping. *ESAIM: M2AN*, 39(3):515–536, 2005.

A Non-dimensional expressions for the numerical fluxes and boundary fluxes

In this section, we detail which fluxes are considered in this article and give their non-dimensional expression.

A.1 The Rusanov flux

The Rusanov numerical flux is given by

$$F^{\mathrm{LF}}\left(\mathbf{W}_i, \mathbf{W}_j, \mathbf{n}\right) = \frac{\mathbf{f}(\mathbf{W}_i) + \mathbf{f}(\mathbf{W}_j)}{2} \cdot \mathbf{n} - \frac{\lambda_{ij}}{2}\left(\mathbf{W}_j - \mathbf{W}_i\right) \tag{35}$$

where $\lambda_{ij} = \max\limits_{\mathbf{W}\in\{\mathbf{W}_i,\mathbf{W}_j\}}(|\lambda_{\pm}(\mathbf{W})|) = \max\limits_{\mathbf{W}\in\{\mathbf{W}_i,\mathbf{W}_j\}}(|\mathbf{u}\cdot\mathbf{n}| + a)$.

This flux can be rephrased in dimensionless variables as

$$\tilde{F}^{\mathrm{LF}}\left(\tilde{\mathbf{W}}_i,\tilde{\mathbf{W}}_j,\mathbf{n},M\right)=\frac{1}{2}\begin{pmatrix}(\tilde{\rho}_i\tilde{\mathbf{u}}_i+\tilde{\rho}_j\tilde{\mathbf{u}}_j)\cdot\mathbf{n}\\ \tilde{\rho}_i\tilde{\mathbf{u}}_i(\tilde{\mathbf{u}}_i\cdot\mathbf{n})+\tilde{\rho}_j\tilde{\mathbf{u}}_j(\tilde{\mathbf{u}}_j\cdot\mathbf{n})+\dfrac{1}{\gamma M^2}(\tilde{p}_i+\tilde{p}_j)\mathbf{n}\end{pmatrix}+\frac{1}{2}\max_{\mathbf{W}\in\{\mathbf{W}_i,\mathbf{W}_j\}}\left(|\tilde{\mathbf{u}}\cdot\mathbf{n}|+\frac{\tilde{a}}{M}\right)\left(\tilde{\mathbf{W}}_i-\tilde{\mathbf{W}}_j\right),$$

to get that

$$\tilde{F}^{\mathrm{LF}}_{\tilde{\rho}}\left(\tilde{\mathbf{W}}_i,\tilde{\mathbf{W}}_j,\mathbf{n},M\right)=\frac{1}{M}\max\left(\tilde{a}\left(\tilde{\rho}_i^{(0)}\right),\tilde{a}\left(\tilde{\rho}_j^{(0)}\right)\right)\left(\tilde{\rho}_i^{(0)}-\tilde{\rho}_j^{(0)}\right)+\mathcal{O}\left(1\right).$$

Moreover, if $\tilde{\rho}_i^{(0)}=\tilde{\rho}_b^{(0)}$, we get (20) where $\tilde{\alpha}_b^{(0)}$ and $\mathbf{D}_{22}(\mathbf{n})$ are given by (24).

A.2 The Roe numerical flux

Defining the Roe average as

$$\rho_{ij}=\sqrt{\rho_i\rho_j},\quad \mathbf{u}_{ij}=\frac{\sqrt{\rho_i}\mathbf{u}_i+\sqrt{\rho_j}\mathbf{u}_j}{\sqrt{\rho_i}+\sqrt{\rho_j}}\quad\text{and}\quad a_{ij}^2=\begin{cases}\dfrac{\Delta p}{\Delta\rho}, & \text{if } \Delta\rho\neq 0,\\ a(\rho_i), & \text{otherwise}\end{cases}\tag{36}$$

where $\Delta(\cdot)=(\cdot)_j-(\cdot)_i$, the Roe numerical flux is defined as

$$\begin{aligned}F^{\mathrm{Roe}}(\mathbf{W}_i,\mathbf{W}_j,\mathbf{n})=&\frac{\mathbf{f}(\mathbf{W}_i)+\mathbf{f}(\mathbf{W}_j)}{2}\cdot\mathbf{n}\\&-\frac{1}{4}\left|\mathbf{u}_{ij}\cdot\mathbf{n}-a_{ij}\right|\left(\Delta\rho-\frac{\rho_{ij}}{a_{ij}}\Delta\left(\mathbf{u}\cdot\mathbf{n}\right)\right)\begin{pmatrix}1\\ \mathbf{u}_{ij}-a_{ij}\mathbf{n}\end{pmatrix}\\&-\frac{1}{2}\left|\mathbf{u}_{ij}\cdot\mathbf{n}\right|\rho_{ij}\begin{pmatrix}0\\ \Delta\mathbf{u}^{\perp}(\mathbf{n})\end{pmatrix}\\&-\frac{1}{4}\left|\mathbf{u}_{ij}\cdot\mathbf{n}+a_{ij}\right|\left(\Delta\rho+\frac{\rho_{ij}}{a_{ij}}\Delta\left(\mathbf{u}\cdot\mathbf{n}\right)\right)\begin{pmatrix}1\\ \mathbf{u}_{ij}+a_{ij}\mathbf{n}\end{pmatrix}\end{aligned}\tag{37}$$

where

$$\mathbf{u}^{\perp}(\mathbf{n}):=\mathbf{u}-(\mathbf{u}\cdot\mathbf{n})\mathbf{n}$$

denotes the tangential component of $\mathbf{u}$ with respect to normal direction $\mathbf{n}$.

The general dimensionless Roe scheme is very complicated, we focus here only on the low Mach number behavior, and therefore express it only in the subsonic case. Then, we have

$$\begin{aligned}\tilde{F}^{\mathrm{Roe}}_{\tilde{\rho}}\left(\tilde{\mathbf{W}}_i,\tilde{\mathbf{W}}_j,\mathbf{n},M\right)=&\frac{\tilde{\rho}_i\tilde{\mathbf{u}}_i+\tilde{\rho}_j\tilde{\mathbf{u}}_j}{2}\cdot\mathbf{n}+M\frac{\tilde{\rho}_{ij}}{2\tilde{a}_{ij}}(\tilde{\mathbf{u}}_{ij}\cdot\mathbf{n})(\tilde{\mathbf{u}}_i-\tilde{\mathbf{u}}_j)\cdot\mathbf{n}+\frac{\tilde{a}_{ij}}{2M}(\tilde{\rho}_i-\tilde{\rho}_j)\\
\tilde{F}^{\mathrm{Roe}}_{\tilde{\rho}\tilde{\mathbf{u}}}\left(\tilde{\mathbf{W}}_i,\tilde{\mathbf{W}}_j,\mathbf{n},M\right)=&\frac{\tilde{\rho}_i(\tilde{\mathbf{u}}_i\cdot\mathbf{n})\tilde{\mathbf{u}}_i+\tilde{\rho}_j(\tilde{\mathbf{u}}_j\cdot\mathbf{n})\tilde{\mathbf{u}}_j}{2}\\&+\frac{\tilde{a}_{ij}}{2M}(\tilde{\rho}_i-\tilde{\rho}_j)\left[\tilde{\mathbf{u}}_{ij}+(\tilde{\mathbf{u}}_{ij}\cdot\mathbf{n})\mathbf{n}\right]\\&+\frac{\tilde{\rho}_{ij}}{2}|\tilde{\mathbf{u}}_{ij}\cdot\mathbf{n}|(\tilde{\mathbf{u}}_i^{\perp}(\mathbf{n})-\tilde{\mathbf{u}}_j^{\perp}(\mathbf{n}))\\&+M\frac{\tilde{\rho}_{ij}(\tilde{\mathbf{u}}_{ij}\cdot\mathbf{n})}{2\tilde{a}_{ij}}[(\tilde{\mathbf{u}}_i-\tilde{\mathbf{u}}_j)\cdot\mathbf{n}]\tilde{\mathbf{u}}_{ij}\\&+\left[\frac{1}{\gamma M^2}\frac{\tilde{p}_i+\tilde{p}_j}{2}+\frac{1}{2M}\tilde{\rho}_{ij}\tilde{a}_{ij}(\tilde{\mathbf{u}}_i-\tilde{\mathbf{u}}_j)\cdot\mathbf{n}\right]\mathbf{n}.\end{aligned}\tag{38}$$

Then, we get

$$\tilde{F}^{\mathrm{Roe}}_{\tilde{\rho}}\left(\tilde{\mathbf{W}}_i,\tilde{\mathbf{W}}_j,\mathbf{n},M\right)=\frac{\tilde{a}_{ij}^{(0)}}{2M}\left(\tilde{\rho}_i^{(0)}-\tilde{\rho}_j^{(0)}\right).$$

Moreover, if $\tilde{\rho}_i^{(0)}=\tilde{\rho}_b^{(0)}$, since the pressure p is a convex function of the density ρ, we get that $\tilde{a}_{ij}^{(0)}=\tilde{a}\left(\tilde{\rho}_b^{(0)}\right)$ and then we obtain (20) where $\tilde{\alpha}_b^{(0)}$ and $\mathbf{D}_{22}(\mathbf{n})$ are given by (25).

A.3 Dimensionless Steger-Warming boundary condition

For inlet and outlet boundary conditions, the Steger-Warming boundary condition is used. Given an external full state $\mathbf{W}_b$, and an interior state $\mathbf{W}_i$, the flux is

$$F^{\mathrm{SW}}(\mathbf{W}_i, \mathbf{W}_b, \mathbf{n}) = A^+(\mathbf{W}_b, \mathbf{n})\mathbf{W}_i + A^-(\mathbf{W}_b, \mathbf{n})\mathbf{W}_b,$$

where A^+ and A^- are respectively the positive and negative parts of the Jacobian matrix of $\mathbf{f}$. For the barotropic Euler system, in the subsonic case $\mathbf{u}_b \cdot \mathbf{n} - a_b < 0 < \mathbf{u}_b \cdot \mathbf{n} + a_b$, this flux is equal to

$$\begin{aligned} F^{\mathrm{SW}}(\mathbf{W}_i, \mathbf{W}_b, \mathbf{n}) =& \frac{1}{2}(\mathbf{u}_b \cdot \mathbf{n} + a_b)\left[\rho_i + \frac{\rho_i}{a_b}(\mathbf{u}_i - \mathbf{u}_b)\cdot\mathbf{n}\right]\begin{pmatrix} 1 \\ \mathbf{u}_b + a_b\mathbf{n} \end{pmatrix} \\ &+ (\mathbf{u}_b \cdot \mathbf{n})^+ \rho_i \begin{pmatrix} 0 \\ (\mathbf{u}_i - \mathbf{u}_b)^\perp(\mathbf{n}) \end{pmatrix} \\ &+ \frac{1}{2}(\mathbf{u}_b \cdot \mathbf{n} - a_b)\rho_b \begin{pmatrix} 1 \\ \mathbf{u}_b - a_b\mathbf{n} \end{pmatrix}. \end{aligned}$$

Then, we get the dimensionless expression as

$$\begin{aligned} \tilde{F}^{\mathrm{SW}}\left(\tilde{\mathbf{W}}_i, \tilde{\mathbf{W}}_b, \mathbf{n}, M\right) =& \frac{1}{2}\tilde{\rho}_i\left(\tilde{\mathbf{u}}_b \cdot \mathbf{n} + \frac{\tilde{a}_b}{M}\right)\left[1 + \frac{M}{\tilde{a}_b}(\tilde{\mathbf{u}}_i - \tilde{\mathbf{u}}_b)\cdot\mathbf{n}\right]\begin{pmatrix} 1 \\ \tilde{\mathbf{u}}_b + \frac{\tilde{a}_b}{M}\mathbf{n} \end{pmatrix} \\ &+ \tilde{\rho}_i(\tilde{\mathbf{u}}_b \cdot \mathbf{n})^+ \begin{pmatrix} 0 \\ (\tilde{\mathbf{u}}_i - \tilde{\mathbf{u}}_b)^\perp(\mathbf{n}) \end{pmatrix} \\ &+ \frac{1}{2}\tilde{\rho}_b\left(\tilde{\mathbf{u}}_b \cdot \mathbf{n} - \frac{\tilde{a}_b}{M}\right)\begin{pmatrix} 1 \\ \tilde{\mathbf{u}}_b - \frac{\tilde{a}_b}{M}\mathbf{n} \end{pmatrix} \end{aligned}$$

that can be rewritten as

$$\begin{aligned} \tilde{F}^{\mathrm{SW}}_{\tilde{\rho}}\left(\tilde{\mathbf{W}}_i, \tilde{\mathbf{W}}_b, \mathbf{n}, M\right) =& \frac{\tilde{\rho}_i\tilde{\mathbf{u}}_i + \tilde{\rho}_b\tilde{\mathbf{u}}_b}{2}\cdot\mathbf{n} + \frac{\tilde{a}_b}{2M}(\tilde{\rho}_i - \tilde{\rho}_b) + M\frac{\tilde{\rho}_i}{2\tilde{a}_b}(\tilde{\mathbf{u}}_b\cdot\mathbf{n})(\tilde{\mathbf{u}}_i - \tilde{\mathbf{u}}_b)\cdot\mathbf{n} \\ \tilde{F}^{\mathrm{SW}}_{\tilde{\rho}\tilde{\mathbf{u}}}\left(\tilde{\mathbf{W}}_i, \tilde{\mathbf{W}}_b, \mathbf{n}, M\right) =& \frac{\tilde{\rho}_i(\tilde{\mathbf{u}}_i\cdot\mathbf{n})\tilde{\mathbf{u}}_i + \tilde{\rho}_b(\tilde{\mathbf{u}}_b\cdot\mathbf{n})\tilde{\mathbf{u}}_b}{2} + \frac{\tilde{a}_b^2}{M^2}\frac{\tilde{\rho}_i + \tilde{\rho}_b}{2} \\ &+ \frac{\tilde{a}_b}{2M}(\tilde{\rho}_i - \tilde{\rho}_b)\left[\tilde{\mathbf{u}}_b + (\tilde{\mathbf{u}}_b\cdot\mathbf{n})\mathbf{n}\right] + \frac{1}{2M}\tilde{\rho}_i\tilde{a}_b\left[(\tilde{\mathbf{u}}_i - \tilde{\mathbf{u}}_b)\cdot\mathbf{n}\right]\mathbf{n} \\ &+ \frac{1}{2}\tilde{\rho}_i|\tilde{\mathbf{u}}_b\cdot\mathbf{n}|(\tilde{\mathbf{u}}_i^\perp(\mathbf{n}) - \tilde{\mathbf{u}}_b^\perp(\mathbf{n})) + \frac{1}{2}\tilde{\rho}_i(\tilde{\mathbf{u}}_b - \tilde{\mathbf{u}}_i)\left[(\tilde{\mathbf{u}}_i - \tilde{\mathbf{u}}_b)\cdot\mathbf{n}\right] \\ &+ M\frac{\tilde{\rho}_i(\tilde{\mathbf{u}}_b\cdot\mathbf{n})}{2\tilde{a}_b}[(\tilde{\mathbf{u}}_i - \tilde{\mathbf{u}}_b)\cdot\mathbf{n}]\tilde{\mathbf{u}}_b. \end{aligned}$$

Then, we get

$$\tilde{F}^{\mathrm{SW}}_{\tilde{\rho}}\left(\tilde{\mathbf{W}}_i, \tilde{\mathbf{W}}_b, \mathbf{n}, M\right) = \frac{\tilde{a}_b^{(0)}}{2M}\left(\tilde{\rho}_i^{(0)} - \tilde{\rho}_b^{(0)}\right) + \mathcal{O}(1).$$

Moreover, if $\tilde{\rho}_i^{(0)} = \tilde{\rho}_b^{(0)}$, we get (22).

A.4 Dimensionless wall boundary condition

For a wall, the following flux is used

$$F^{\mathrm{wall}}(\mathbf{W}_i, \mathbf{n}) = F(\mathbf{W}_i, \breve{\mathbf{W}}_i, \mathbf{n}_{ij})$$

where the flux F corresponds to the flux taken in the domain and $\breve{\mathbf{W}}_i$ is obtained from the transformation of $\mathbf{W}_i$: $\breve{\mathbf{W}}_i = (\mathrm{I}_{d+1} - P_{\mathrm{wall}}(\mathbf{n}))\mathbf{W}_i$ with

$$P_{\mathrm{wall}}(\mathbf{n}) = \begin{pmatrix} 0 & 0 \\ 0 & 2\mathbf{n}\mathbf{n}^T \end{pmatrix}.$$

In the case of a Rusanov flux, we get

$$\tilde{F}^{\mathrm{wall,Rusanov}}\left(\tilde{\mathbf{W}}_i, \mathbf{n}, M\right) = \begin{pmatrix} 0 \\ \frac{1}{\gamma M^2}\tilde{p}_i\mathbf{n} + \tilde{\rho}_i(\tilde{\mathbf{u}}_i\cdot\mathbf{n})^2\mathbf{n} + \left(|\tilde{\mathbf{u}}_i\cdot\mathbf{n}| + \frac{\tilde{a}_i}{M}\right)\tilde{\rho}_i(\tilde{\mathbf{u}}_i\cdot\mathbf{n})\mathbf{n} \end{pmatrix}$$

so that $\tilde{F}_{\tilde{\rho}}^{\text{wall,Rusanov}} = 0$. Moreover, if $\tilde{\rho}_i^{(0)} = \tilde{\rho}_b^{(0)}$ is ensured, $\tilde{F}_{\tilde{\rho}\tilde{\mathbf{u}}}^{\text{wall,Rusanov}}$ satisfies (21) because $\tilde{a}_i^{(0)} = \tilde{a}_b^{(0)}$.

In the case of the Roe flux, we get

$$\tilde{F}^{\text{wall,Roe}}\left(\tilde{\mathbf{W}}_i, \mathbf{n}, M\right) = \begin{pmatrix} 0 \\ \dfrac{1}{\gamma M^2}\tilde{p}_i\mathbf{n} + \tilde{\rho}_i(\tilde{\mathbf{u}}_i\cdot\mathbf{n})^2\mathbf{n} + \dfrac{1}{M}\tilde{\rho}_i\tilde{a}_i(\tilde{\mathbf{u}}_i\cdot\mathbf{n})\mathbf{n} \end{pmatrix}$$

and the same result is obtained because order $1/M^2$ and $1/M$ are the same as the Rusanov flux.

B Proof of the propositions on continuous and discrete Hodge-Helmholtz decompositions

B.1 Decomposition in the continuous case

In this subsection, we prove Proposition 1.

The decomposition can be written as

$$\mathbf{u} = \nabla_{\mathbf{x}}\varphi + \mathbf{curl}_{\mathbf{x}}\boldsymbol{\Psi}.$$

Taking the divergence of the equality gives

$$\Delta_{\mathbf{x}}\varphi = \text{div}_{\mathbf{x}}\mathbf{u}.$$

This equation is multiplied by a regular test function g and integrated on Ω

$$\int_\Omega g\Delta_{\mathbf{x}}\varphi = \int_\Omega g\text{div}_{\mathbf{x}}\mathbf{u}.$$

The left hand side is integrated by parts as follows

$$\begin{aligned}\int_\Omega g\Delta_{\mathbf{x}}\varphi &= \int_\Omega g\text{div}_{\mathbf{x}}\left(\nabla_{\mathbf{x}}\varphi\right)\\ &= \int_\Omega \text{div}_{\mathbf{x}}\left(g\nabla_{\mathbf{x}}\varphi\right) - \int_\Omega \nabla_{\mathbf{x}}g\cdot\nabla_{\mathbf{x}}\varphi\\ &= \int_{\partial\Omega} g\nabla_{\mathbf{x}}\varphi\cdot\mathbf{n} - \int_\Omega \nabla_{\mathbf{x}}g\cdot\nabla_{\mathbf{x}}\varphi\\ &= \int_{\partial\Omega} g\left(\mathbf{u}\cdot\mathbf{n} - \mathbf{u}_b\cdot\mathbf{n}\right) - \int_\Omega \nabla_{\mathbf{x}}g\cdot\nabla_{\mathbf{x}}\varphi.\end{aligned}$$

Therefore the following variational formulation is found

$$\text{Find } \varphi\in H^1(\Omega)\quad \forall g\in H^1(\Omega)\qquad \int_\Omega \nabla_{\mathbf{x}}g\cdot\nabla_{\mathbf{x}}\varphi = \int_{\partial\Omega} g\left(\mathbf{u}\cdot\mathbf{n} - \mathbf{u}_b\cdot\mathbf{n}\right) - \int_\Omega g\text{div}_{\mathbf{x}}\mathbf{u}. \tag{39}$$

Note that all the integral of the right hand side have a sense, because if $\mathbf{u}\in H^1(\Omega)$, then its divergence is in $H^{-1}(\Omega)$. The variational problem (39) has a unique solution up to a constant provided Ω is simply connex. By taking the gradient of φ, we find the component $\mathbf{u}_\varphi$. By defining

$$\mathbf{u}_{\boldsymbol{\Psi}} = \mathbf{u} - \mathbf{u}_\varphi,$$

existence of the decomposition is found. Let's now proof the uniqueness. Suppose that we have two decompositions

$$\mathbf{u} = \mathbf{u}_\varphi^1 + \mathbf{u}_{\boldsymbol{\Psi}}^1 = \mathbf{u}_\varphi^2 + \mathbf{u}_{\boldsymbol{\Psi}}^2,$$

with the following boundary conditions

$$\mathbf{u}_\varphi^1\cdot\mathbf{n} = \mathbf{u}_\varphi^2\cdot\mathbf{n} = \mathbf{u}\cdot\mathbf{n} - \mathbf{u}_b\cdot\mathbf{n},$$

then

$$\mathbf{u}_\varphi^1 - \mathbf{u}_\varphi^2 = \mathbf{u}_{\boldsymbol{\Psi}}^2 - \mathbf{u}_{\boldsymbol{\Psi}}^1. \tag{40}$$

We denote by φ^1 (resp. φ^2) a potential such that $\nabla_{\mathbf{x}}\varphi^1 = \mathbf{u}_\varphi^1$ (resp. $\nabla_{\mathbf{x}}\varphi^2 = \mathbf{u}_\varphi^2$). By taking the divergence of the equality, we find that $\varphi^1 - \varphi^2$ is such that

$$\begin{cases}\Delta_{\mathbf{x}}\left(\varphi^1 - \varphi^2\right) = 0 & \text{in } \Omega,\\ \nabla_{\mathbf{x}}\left(\varphi^1 - \varphi^2\right)\cdot\mathbf{n} = 0 & \text{in } \partial\Omega.\end{cases}$$

As Ω is simply connex, a constant K exists such that $\varphi^1 - \varphi^2 = K$. This leads to $\mathbf{u}_\varphi^1 = \mathbf{u}_\varphi^2$. Following (40), $\mathbf{u}_{\boldsymbol{\Psi}}^1 = \mathbf{u}_{\boldsymbol{\Psi}}^2$, so that uniqueness is proven.

B.2 Long time behaviour of the continuous wave system

The aim of this section is to prove Proposition 2. We first need to prove the following lemma:

Lemma 1. *Consider the wave system (13) with initial velocity $\widehat{\mathbf{u}}_0$, and with boundary conditions weakly defined by (14b) for wall, and by (14c) for inlet/outlet. Consider now a stationary state $\mathbf{U}^\infty = (\widehat{p}^\infty, \widehat{\mathbf{u}}^\infty)$ that $\widehat{\mathbf{u}}^\infty$ is divergence free and such that $\widehat{p}^\infty$ is uniformly equal to $\widehat{p}_b$, and such that $\widehat{\mathbf{u}}^\infty \cdot \mathbf{n} = 0$ on walls and $\widehat{\mathbf{u}}^\infty \cdot \mathbf{n} = \widehat{\mathbf{u}}_b \cdot \mathbf{n}$ on inlet/outlet. We define the relative energy as*

$$E_{\mathbf{U}^\infty}(\mathbf{U}) := \frac{\widehat{\rho_0}^2 \widehat{c_0}^2}{2} \left(\widehat{p} - \widehat{p}^\infty\right)^2 + \frac{1}{2} \left(\widehat{\mathbf{u}} - \widehat{\mathbf{u}}^\infty\right)^2.$$

Then the volumic average of the relative energy is a Liapunov functional.

Proof. Consider the weak formulation of the wave system

$$\forall g, \mathbf{g} \begin{cases} \displaystyle\int_\Omega g \partial_t \widehat{p} - \int_\Omega \frac{1}{\widehat{\rho_0}} \widehat{\mathbf{u}} \cdot \nabla_{\mathbf{x}} g + \int_{\partial\Omega} g \left[\frac{1}{\widehat{\rho_0}} \widehat{\mathbf{u}} \cdot \mathbf{n}\right]_{\text{wall/SW}} = 0, \\ \displaystyle\int_\Omega \mathbf{g} \cdot \partial_t \widehat{\mathbf{u}} - \int_\Omega \widehat{\kappa_0} \widehat{p} \operatorname{div}_{\mathbf{x}} \mathbf{g} + \int_{\partial\Omega} \mathbf{g} \cdot \left[\widehat{\kappa_0} \widehat{p} \mathbf{n}\right]_{\text{wall/SW}} = 0. \end{cases}$$

Now, we set $\mathbf{g} = \widehat{\mathbf{u}} - \widehat{\mathbf{u}}^\infty$ and $g = \widehat{p} - \widehat{p}^\infty$, multiply the equation of pressure by $\widehat{\rho_0}^2 \widehat{c_0}^2$, and add the two equations, for finding

$$\begin{aligned} &\int_\Omega \partial_t E_{\mathbf{U}^\infty}(\mathbf{U}) - \int_\Omega \widehat{\rho_0} \widehat{c_0}^2 \operatorname{div}_{\mathbf{x}} \left(\widehat{p} \widehat{\mathbf{u}}\right) \\ &\qquad + \int_{\partial\Omega} \widehat{\rho_0}^2 \widehat{c_0}^2 \left(\widehat{p} - \widehat{p}^\infty\right) \left[\frac{1}{\widehat{\rho_0}} \widehat{\mathbf{u}} \cdot \mathbf{n}\right]_{\text{wall/SW}} + \left(\widehat{\mathbf{u}} - \widehat{\mathbf{u}}^\infty\right) \cdot \left[\widehat{\kappa_0} \widehat{p} \mathbf{n}\right]_{\text{wall/SW}} = 0. \end{aligned}$$

The second volumic integral can be integrated, which gives

$$\begin{aligned} &\int_\Omega \partial_t E_{\mathbf{U}^\infty}(\mathbf{U}) - \int_{\partial\Omega} \widehat{\rho_0} \widehat{c_0}^2 \widehat{p} \widehat{\mathbf{u}} \cdot \mathbf{n} \\ &\qquad + \int_{\partial\Omega} \left(\widehat{\rho_0}^2 \widehat{c_0}^2 \left(\widehat{p} - \widehat{p}^\infty\right) \left[\frac{1}{\widehat{\rho_0}} \widehat{\mathbf{u}} \cdot \mathbf{n}\right]_{\text{wall/SW}} + \left(\widehat{\mathbf{u}} - \widehat{\mathbf{u}}^\infty\right) \cdot \left[\widehat{\kappa_0} \widehat{p} \mathbf{n}\right]_{\text{wall/SW}} \right) = 0. \end{aligned}$$

The boundary flux on walls is given by (14b). Moreover, on the wall boundary, we have $\widehat{\mathbf{u}}^\infty \cdot \mathbf{n} = 0$. This means that on the wall boundary

$$\begin{aligned} &- \widehat{\rho_0} \widehat{c_0}^2 \widehat{p} \widehat{\mathbf{u}} \cdot \mathbf{n} + \widehat{\rho_0}^2 \widehat{c_0}^2 \left(\widehat{p} - \widehat{p}^\infty\right) \left[\frac{1}{\widehat{\rho_0}} \widehat{\mathbf{u}} \cdot \mathbf{n}\right]_{\text{wall}} + \widehat{\mathbf{u}} \cdot \left[\widehat{\kappa_0} \widehat{p} \mathbf{n}\right]_{\text{wall}} \\ &= - \widehat{\rho_0} \widehat{c_0}^2 \widehat{p} \widehat{\mathbf{u}} \cdot \mathbf{n} + \widehat{\rho_0} \widehat{c_0}^2 \left(\widehat{p} + \widehat{c_0} \widehat{\mathbf{u}} \cdot \mathbf{n}\right) \widehat{\mathbf{u}} \cdot \mathbf{n} \\ &= \widehat{\rho_0} \widehat{c_0}^2 \left(\widehat{\mathbf{u}} \cdot \mathbf{n}\right)^2 \geqslant 0, \end{aligned}$$

whereas for the inlet/outlet, the boundary flux (14c) can be written as

$$\begin{bmatrix} \frac{1}{\widehat{\rho_0}} \widehat{\mathbf{u}} \cdot \mathbf{n} \\ \widehat{\kappa_0} \widehat{p} \mathbf{n} \end{bmatrix}_{\text{SW}} = \begin{pmatrix} \frac{1}{2\widehat{\rho_0}} \widehat{\mathbf{u}} \cdot \mathbf{n} \\ \frac{\widehat{\kappa_0}}{2} \widehat{p} \mathbf{n} \end{pmatrix} + \begin{pmatrix} \frac{1}{2\widehat{\rho_0}} \widehat{\mathbf{u}}_b \cdot \mathbf{n} + \frac{\widehat{c_0}}{2} \left(\widehat{p} - \widehat{p}_b\right) \\ \left(\frac{\widehat{\kappa_0}}{2} \widehat{p}_b + \frac{\widehat{c_0}}{2} \left(\widehat{\mathbf{u}} \cdot \mathbf{n} - \widehat{\mathbf{u}}_b \cdot \mathbf{n}\right)\right) \mathbf{n} \end{pmatrix},$$

then

$$\begin{aligned} &- \widehat{\rho_0} \widehat{c_0}^2 \widehat{p} \widehat{\mathbf{u}} \cdot \mathbf{n} + \widehat{\rho_0}^2 \widehat{c_0}^2 \left(\widehat{p} - \widehat{p}^\infty\right) \left[\frac{1}{\widehat{\rho_0}} \widehat{\mathbf{u}} \cdot \mathbf{n}\right]_{\text{SW}} + \left(\widehat{\mathbf{u}} - \widehat{\mathbf{u}}^\infty\right) \cdot \left[\widehat{\kappa_0} \widehat{p} \mathbf{n}\right]_{\text{SW}} \\ &= - \widehat{\rho_0} \widehat{c_0}^2 \widehat{p} \widehat{\mathbf{u}} \cdot \mathbf{n} + \widehat{\rho_0}^2 \widehat{c_0}^2 \left(\widehat{p} - \widehat{p}^\infty\right) \left(\frac{1}{2\widehat{\rho_0}} \widehat{\mathbf{u}} \cdot \mathbf{n} + \frac{1}{2\widehat{\rho_0}} \widehat{\mathbf{u}}_b \cdot \mathbf{n} + \frac{\widehat{c_0}}{2} \left(\widehat{p} - \widehat{p}_b\right)\right) \\ &\qquad + \left(\widehat{\mathbf{u}} - \widehat{\mathbf{u}}^\infty\right) \cdot \mathbf{n} \left(\frac{\widehat{\kappa_0}}{2} \widehat{p} + \frac{\widehat{\kappa_0}}{2} \widehat{p}_b + \frac{\widehat{c_0}}{2} \left(\widehat{\mathbf{u}} \cdot \mathbf{n} - \widehat{\mathbf{u}}_b \cdot \mathbf{n}\right)\right) \\ &= - \widehat{\rho_0} \widehat{c_0}^2 \widehat{p} \widehat{\mathbf{u}} \cdot \mathbf{n} + \widehat{\rho_0}^2 \widehat{c_0}^2 \left(\widehat{p} - \widehat{p}^\infty\right) \left(\frac{1}{2\widehat{\rho_0}} \widehat{\mathbf{u}} \cdot \mathbf{n} + \frac{1}{2\widehat{\rho_0}} \widehat{\mathbf{u}}_b \cdot \mathbf{n} + \frac{\widehat{c_0}}{2} \left(\widehat{p} - \widehat{p}_b\right)\right) \\ &\qquad + \left(\widehat{\mathbf{u}} - \widehat{\mathbf{u}}^\infty\right) \cdot \mathbf{n} \left(\frac{\widehat{\kappa_0}}{2} \widehat{p} + \frac{\widehat{\kappa_0}}{2} \widehat{p}_b + \frac{\widehat{c_0}}{2} \left(\widehat{\mathbf{u}} \cdot \mathbf{n} - \widehat{\mathbf{u}}_b \cdot \mathbf{n}\right)\right) \\ &= \frac{\widehat{\rho_0} \widehat{c_0}^3}{2} \left(\widehat{p} - \widehat{p}_b\right)^2 + \frac{\widehat{c_0}}{2} \left(\widehat{\mathbf{u}} \cdot \mathbf{n} - \widehat{\mathbf{u}}_b \cdot \mathbf{n}\right)^2 \geqslant 0. \end{aligned}$$

We finally find

$$\partial_t \left(\int_\Omega E_{\mathbf{U}^\infty}(\mathbf{U}) \right) \leqslant 0,$$

which ends the proof. □

We now prove a second lemma

Lemma 2. *If $(\widehat{p}, \widehat{\mathbf{u}})$ is the solution of the wave system (13), and if we consider the Hodge-Helmholtz decomposition (15) of $\widehat{\mathbf{u}}$, then $\widehat{\mathbf{u}}_{\mathbf{\Psi}}$ is constant.*

Proof. By integrating by parts in (39) the integral involving the divergence, we find the following variational formulation

$$\text{Find } \varphi \in H^1(\Omega) \quad \forall g \in H^1(\Omega) \qquad \int_\Omega \nabla_{\mathbf{x}} g \cdot \nabla_{\mathbf{x}} \varphi = \int_\Omega \widehat{\mathbf{u}} \cdot \nabla_{\mathbf{x}} g - \int_{\partial\Omega} g \widehat{\mathbf{u}}_b \cdot \mathbf{n}. \tag{41}$$

Taking the derivative in time gives

$$\forall g \in H^1(\Omega) \qquad \int_\Omega \nabla_{\mathbf{x}} g \cdot \partial_\tau \left(\nabla_{\mathbf{x}} \varphi \right) = \int_\Omega \partial_\tau \widehat{\mathbf{u}} \cdot \nabla_{\mathbf{x}} g = - \int_\Omega \widehat{\kappa_0} \nabla_{\mathbf{x}} \widehat{p} \cdot \nabla_{\mathbf{x}} g,$$

which leads to

$$\forall g \in H^1(\Omega) \qquad \int_\Omega \nabla_{\mathbf{x}} g \cdot (\partial_\tau \widehat{\mathbf{u}}_\varphi + \widehat{\kappa_0} \nabla_{\mathbf{x}} \widehat{p}) = 0.$$

As $\partial_\tau \widehat{\mathbf{u}}_\varphi + \widehat{\kappa_0} \nabla_{\mathbf{x}} \widehat{p}$ is the gradient of $\partial_\tau \varphi + \widehat{\kappa_0} \widehat{p}$, this means that

$$\partial_\tau \widehat{\mathbf{u}}_\varphi + \widehat{\kappa_0} \nabla_{\mathbf{x}} \widehat{p} = 0,$$

so that $\partial_\tau \widehat{\mathbf{u}}_{\mathbf{\Psi}} = 0$. □

We can now prove Proposition 2. Considering Lemma 1, it is clear that the pressure at infinity is uniform, equal to $\widehat{p}_b$, and that the velocity at infinity is divergence free, so that $\widehat{\mathbf{u}}_\varphi$ is 0 at infinity. Then, following Lemma 2, $\widehat{\mathbf{u}}_{\mathbf{\Psi}}$ is constant, so that the limit of $\widehat{\mathbf{u}}$ at infinite time is equal to $\widehat{\mathbf{u}}_{\mathbf{\Psi}}(0)$.

B.3 Discrete decomposition on triangular meshes

In this section, Proposition 5 is proven.

Let $\mathbf{u}_h \in \mathbb{R}^{2N_{\text{Cells}}}$. We first remark that the variational formulation in the continuous case (39) can be transformed, by using the Green formula on the last integral of the right hand side as

$$\text{Find } \varphi \in H^1(\Omega) \quad \forall g \in H^1(\Omega) \qquad \int_\Omega \nabla_{\mathbf{x}} g \cdot \nabla_{\mathbf{x}} \varphi = - \int_{\partial\Omega} g \mathbf{u}_b \cdot \mathbf{n} + \int_\Omega \nabla_{\mathbf{x}} g \cdot \mathbf{u}. \tag{42}$$

This suggests to define φ_h and so $\mathcal{P}_h^\varphi [\mathbf{u}_h] = \nabla \varphi_h$ as the solution of the following discrete variational problem

$$\text{Find } \varphi_h \in W_h \quad \forall g_h \in W_h \qquad \sum_K \int_K \nabla_{\mathbf{x}} g_h \cdot \nabla_{\mathbf{x}} \varphi_h = \sum_K \int_K \mathbf{u}_h \cdot \nabla g_h - \sum_{f \in \mathcal{F}_{\text{wall/SW}}} \int_f g_h \mathbf{u}_b \cdot \mathbf{n}. \tag{43}$$

We will now prove that $\mathbf{u}_h^\psi := \mathbf{u}_h - \nabla \varphi_h \in Z_h$ and later we will prove that all element of Z_h can be written as the curl of an element of V_h. For all $g_h \in W_h$, we have

$$\begin{aligned}
\sum_{f \in \mathcal{F}_{\text{wall/SW}}} \int_f g_h \mathbf{u}_b \cdot \mathbf{n} &= \sum_K \int_K (\mathbf{u}_h - \nabla \varphi_h) \cdot \nabla g_h \\
&= \sum_K \int_K \mathbf{u}_h^\psi \cdot \nabla g_h \\
&= \sum_K \int_K \text{div}_{\mathbf{x}}(\mathbf{u}_h^\psi g_h) - \sum_K \int_K g_h \text{div}_{\mathbf{x}}(\mathbf{u}_h^\psi) \\
&= \sum_K \int_{\partial K} g_h \mathbf{u}_h^\psi \cdot \mathbf{n} \\
&= \sum_{f \in \mathcal{F}_{\text{int}}} \int_f [\![g_h \mathbf{u}_h^\psi \cdot \mathbf{n}]\!] + \sum_{f \in \mathcal{F}_{\text{wall/SW}}} \int_f g_h \mathbf{u}_h^\psi \cdot \mathbf{n} \\
&= \sum_{f \in \mathcal{F}_{\text{int}}} \int_f \{\!\{ g_h \}\!\} [\![\mathbf{u}_h^\psi \cdot \mathbf{n}]\!] + \sum_{f \in \mathcal{F}_{\text{int}}} \int_f [\![g_h]\!] \left\{\!\!\left\{ \mathbf{u}_h^\psi \cdot \mathbf{n} \right\}\!\!\right\} + \sum_{f \in \mathcal{F}_{\text{wall/SW}}} \int_f g_h \mathbf{u}_h^\psi \cdot \mathbf{n}.
\end{aligned}$$

As $\mathbf{u}_h^\psi$ is piecewise constant, $\left\{\!\!\left\{ \mathbf{u}_h^\psi \cdot \mathbf{n} \right\}\!\!\right\}$ is constant along the face, which means that on all interior faces $f \in \mathcal{F}_{\text{int}}$,

$$\int_f \left\{\!\!\left\{ \mathbf{u}_h^\psi \cdot \mathbf{n} \right\}\!\!\right\} [\![g_h]\!]$$

is proportional to

$$\int_f [\![g_h]\!],$$

which is 0 since g_h is in W_h. Then, $\mathbf{u}_h^\psi \in Z_h$ and the application

$$\begin{aligned} L: \quad W_h \times Z_h &\longrightarrow \mathbb{R}^{2N_{\text{Cells}}} \\ (\varphi_h, \mathbf{u}_h^\psi) &\longmapsto \nabla\varphi_h + \mathbf{u}_h^\psi \end{aligned}$$

is surjective. Moreover, since any $\varphi_h \in W_h$ is completely and uniquely determined by its value at the $\#\mathcal{F}$ independent face midpoint of the mesh, we have $\dim(W_h) = \#\mathcal{F}$. Using the definition of Z_h, we get that $\dim(Z_h) = 2N_{\text{Cells}} - \#\mathcal{F}_{\text{wall/SW}} - \#\mathcal{F}_{\text{int}} = 2N_{\text{Cells}} - \#\mathcal{F}$ and then,

$$\dim(W_h) + \dim(Z_h) = 2N_{\text{Cells}},$$

so that the application L is bijective and the decomposition is unique.
We now prove that $Z_h = \nabla \times V_h^{\text{boundary}}$ where

$$V_h^{\text{boundary}} := \left\{ \psi_h \in V_h \;\middle|\; \int_\Omega \psi_h = 0 \text{ and } \forall f \in \mathcal{F}_{\text{wall/SW}},\ (\nabla \times \psi_h) \cdot \mathbf{n}_f = \mathbf{u}_b \cdot \mathbf{n}_f \right\}.$$

It is easy to prove that the application

$$\begin{aligned} G: \quad V_h^{\text{boundary}} &\longrightarrow Z_h \\ \psi_h &\longmapsto \nabla \times \psi_h \end{aligned}$$

is well defined and injective. Since any $\psi_h \in V_h$ is completely and uniquely determined by its value at the S independent nodes of the mesh, we have $\dim(V_h) = S + r$ where r is the number of holes of the mesh. Since $\#\mathcal{F}_{\text{wall/SW}} = S_{\text{wall/SW}}$ where $S_{\text{wall/SW}}$ is the number of nodes on the boundary, we have

$$\dim(V_h^{\text{boundary}}) = S + r - S_{\text{wall/SW}} - 1 = S_{\text{int}} + r - 1$$

where S_{int} is the number of interior nodes. Since $S + N_{\text{Cells}} = \#\mathcal{F} + 1 - r$ [28, Lemma 2.1] and since $3N_{\text{Cells}} = 2\#\mathcal{F}_{\text{int}} + \#\mathcal{F}_{\text{wall/SW}}$ (because we consider a triangular mesh), we get

$$\begin{aligned} N_{\text{Cells}} &= 2\#\mathcal{F}_{\text{int}} + \#\mathcal{F}_{\text{wall/SW}} - 2N_{\text{Cells}} \\ &= 2(\#\mathcal{F} - N_{\text{Cells}}) - \#\mathcal{F}_{\text{wall/SW}} \\ &= 2(S + r - 1) - \#\mathcal{F}_{\text{wall/SW}} \\ &= 2(r-1) + S + S_{\text{int}}, \end{aligned}$$

so that

$$\begin{aligned} S_{\text{int}} + r - 1 &= N_{\text{Cells}} - (S + r - 1) \\ &= N_{\text{Cells}} - (\#\mathcal{F} - N_{\text{Cells}}) \\ &= 2N_{\text{Cells}} - \#\mathcal{F}, \end{aligned}$$

and $\dim(V_h^{\text{boundary}}) = \dim(Z_h)$.

B.4 Long time behaviour of the discrete wave system with Godunov' scheme on triangular meshes

We prove Proposition 6. Assume that $\mathbf{U}_h^0 = (\widehat{p}_h^0, \widehat{\mathbf{u}}_h^0)$ is such that $\widehat{p}_h^0 = \widehat{p}_b$ and $\mathcal{P}_h^\varphi\left[\widehat{\mathbf{u}}_h^0\right] = 0$. Using Proposition 5, we have $\widehat{\mathbf{u}}_h^0 = \mathcal{P}_h^\Psi\left[\widehat{\mathbf{u}}_h^0\right] \in Z_h$. Then, using (19) with stabilization (25) and the definition of Z_h (29), we get for all $j \in \mathcal{V}_{\text{int}}(i)$,

$$D(\mathbf{n}_{ij})\left(\mathbf{U}_j^0 - \mathbf{U}_i^0\right) = \frac{\widehat{c}_0}{2}\begin{pmatrix} \widehat{p}_j^0 - \widehat{p}_i^0 \\ \left((\widehat{\mathbf{u}}_j^0 - \widehat{\mathbf{u}}_i^0) \cdot \mathbf{n}_{ij}\right)\mathbf{n}_{ij} \end{pmatrix} = 0 \quad \text{and} \quad A(\mathbf{n}_{ij})\mathbf{U}_i^0 = A(\mathbf{n}_{ij})\mathbf{U}_j^0,$$

for all $j \in \mathcal{V}_{\text{wall}}(i)$,

$$\begin{aligned}
\left(A(\mathbf{n}_{ij}) - 2A^-(\mathbf{n}_{ij})P_{\text{wall}}(\mathbf{n}_{ij})\right)\mathbf{U}_i^0 &= \begin{pmatrix} 0 & -\frac{1}{\widehat{\rho_0}}\mathbf{n}_{ij}^T \\ \widehat{\kappa_0}\mathbf{n}_{ij} & 2\widehat{c_0}\mathbf{n}_{ij}\mathbf{n}_{ij}^T \end{pmatrix}\mathbf{U}_i^0 \\
&= \begin{pmatrix} -\frac{1}{\widehat{\rho_0}}\widehat{\mathbf{u}}_i^0 \cdot \mathbf{n}_{ij} \\ \widehat{\kappa_0}\widehat{p}_i^0\mathbf{n}_{ij} + 2\widehat{\mathbf{u}}_i^0 \cdot \mathbf{n}_{ij} \end{pmatrix} \\
&= \begin{pmatrix} 0 \\ \widehat{\kappa_0}\widehat{p}_i^0\mathbf{n}_{ij} \end{pmatrix} \\
&= A(\mathbf{n}_{ij})\mathbf{U}_i^0,
\end{aligned}$$

and for all $j \in \mathcal{V}_{\text{SW}}(i)$, $A(\mathbf{n}_{ij})\mathbf{U}_i^0 = A(\mathbf{n}_{ij})\mathbf{U}_b$ and

$$\begin{aligned}
\left(A^+(\mathbf{n}_{ij}) - A^-(\mathbf{n}_{ij})\right)\left(\mathbf{U}_b - \mathbf{U}_i^0\right) &= \widehat{c_0}\begin{pmatrix} 1 & 0 \\ 0 & \mathbf{n}_{ij}\mathbf{n}_{ij}^T \end{pmatrix}\left(\mathbf{U}_b - \mathbf{U}_i^0\right) \\
&= \widehat{c_0}\begin{pmatrix} \widehat{p}_b - \widehat{p}_i^0 \\ \left((\widehat{\mathbf{u}}_b - \widehat{\mathbf{u}}_i^0) \cdot \mathbf{n}_{ij}\right)\mathbf{n}_{ij} \end{pmatrix} \\
&= 0,
\end{aligned}$$

so that (19) becomes

$$\frac{\mathbf{U}_i^1 - \mathbf{U}_i^0}{\delta t} + \frac{1}{|\tilde{\Omega}_i|}\sum_{j\in\mathcal{V}(i)} |\tilde{\Gamma}_{ij}| A(\mathbf{n}_{ij})\mathbf{U}_i^0 = 0.$$

Since $\sum_{j\in\mathcal{V}(i)} |\tilde{\Gamma}_{ij}|\mathbf{n}_{ij} = 0$, we get that $\mathbf{U}_i^1 = \mathbf{U}_i^0$.